Efficiency of Fiber Reinforcement in Ultra-high Performance Concrete

Final Report
November 2025

Principal Investigator: Kay Wille, Ph. D., Professor

School of Civil and Environmental Engineering
University of Connecticut

Authors
Mandip Dahal, Ph.D. Student
Kay Wille, Ph. D., Professor

Sponsored By
Transportation Infrastructure Durability Center

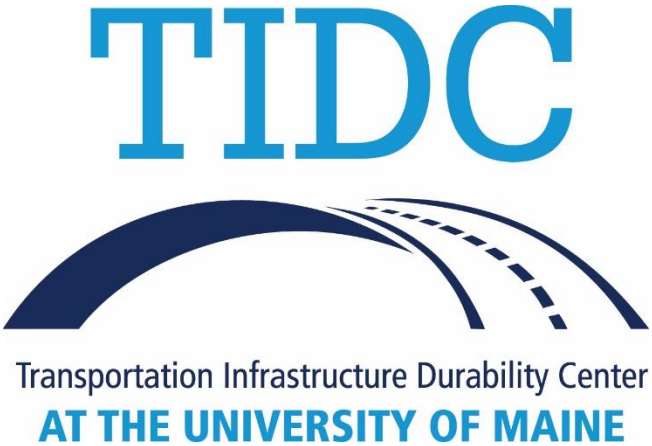

A report from
University of Connecticut
School of Civil and Environmental Engineering
261 Glenbrook Road, Unit 3037, Storrs, CT 06269-3037
Phone: (860) 486-2992
Website: https://cee.engr.uconn.edu/

About the Transportation Infrastructure Durability Center

The Transportation Infrastructure Durability Center (TIDC) is the 2018 US DOT Region 1 (New England) University Transportation Center (UTC) located at the University of Maine Advanced Structures and Composites Center. TIDC's research focuses on efforts to improve the durability and extend the life of transportation infrastructure in New England and beyond through an integrated collaboration of universities, state DOTs, and industry. The TIDC is comprised of six New England universities, the University of Maine (lead), the University of Connecticut, the University of Massachusetts Lowell, the University of Rhode Island, the University of Vermont, and Western New England University.

U.S. Department of Transportation (US DOT) Disclaimer

Acknowledgements

Funding for this research is provided by the Transportation Infrastructure Durability Center at the University of Maine under grant 69A3551847101 from the U.S. Department of Transportation's University Transportation Centers Program. The principal and co-principal investigator of the project would like to gratefully acknowledge and thank the following individuals and organizations whose support (financial, material, and/or in-kind) assisted in this research and significantly contributed to the success of the project:

Graduate and undergraduate assistants involved in this project:
Mandip Dahal, Ph.D. student
Max Raha, Undergraduate student
Zita Boutin-Johnson, Undergraduate student (REU program)

Project Technical Champions:
The following technical champions for providing valuable comments during the course of this project:

Messrs. Andrew Cardinali, P.E. and Bao Chuong, P.E. Connecticut Department of Transportation, Newington, CT

State Department of Transportation:

The Connecticut Department of Transportation, Newington, Connecticut, for their in-kind support.

Industry for supplying materials:

Bekaert fiber, HiPer fiber, Ductal, Helix steel, Boral Flyash, Lafarge Holcim Cement, Norchem, Elkem, Tilcon and Chryso Inc.

Last, but not least, the University of Connecticut, its School of Civil and Environmental Engineering, Advanced Cementitious Materials and Composites (ACMC) lab, and Connecticut Transportation Institute (CTI) for cost share, in-kind support, laboratory facilities, and project administration help.

Technical Report Documentation Page

1. Report No.	2. Government Accession No.	3. Recipient Catalog No.
4 Title and Subtitle 2.20 Efficiency of Fiber Reinforcement in Ultra-high Performance Concrete		**5 Report Date** 11/26/2025 **6 Performing Organization Code**
7. Author(s) Mandip Dahal Kay Wille - https://orcid.org/0000-0001-7398-3456		**8 Performing Organization Report No.**
9 Performing Organization Name and Address University of Connecticut 261 Glenbrook Rd Storrs, CT 06269-3037		**10 Work Unit No. (TRAIS)** **11 Contract or Grant No.**
12 Sponsoring Agency Name and Address U.S. DOT Region 1 University Transportation Center (UTC) -Transportation Infrastructure Durability Center (TIDC), ASCC, University of Maine, 35 Flagstaff Rd., Orono, Maine, U.S.A.		**13 Type of Report and Period Covered** Final Report 10/01/2023-07/31/2025 **14 Sponsoring Agency Code**
15 Supplementary Notes		

16 Abstract

This report is based on the findings to advance the understanding of fiber efficiency in ultra-high performance concrete. The work begins with single-fiber pullout tests on both commercial and newly proposed bundled steel fibers, introducing a slip-hardening factor to better characterize bond performance. It then expands to a comprehensive program involving nine fiber geometries at multiple volume fractions, through which new fiber efficiency and utilization factors are developed to quantify how fiber geometry, strength, aspect ratio, and dosage interact within the UHPC matrix. Finally, long-term direct tensile tests on UHPC specimens naturally cured for 13.5 years demonstrate the sustained contribution of fibers to tensile strength and ductility over time.

17 Key Words	18 Distribution Statement
Single fiber pullout test, Direct tensile test, Bundled fibers, Fiber efficiency factor, Fiber utilization factor, ultra high performance concrete	This document is available for public reference after the acceptance of the scientific articles are published.

19 Security Classification (of this report)	20 Security Classification (of this page)	21 No. of pages	22 Price
Unclassified	Unclassified	44	

Form DOT F 1700.7 (8-72)

Contents

List of Figures 5
List of Tables 6
List of Key Terms 7
Abstract 8
Chapter 1: Introduction and Background 9
1.1 Project Motivation 9
1.2 Research, Objectives, and Tasks 10
1.3 Report Overview 11
Chapter 2: Methodology 12
2.1 Materials, mix design and sample preparation 12
2.2 Test Procedure and Analysis 14
Chapter 3: Results and Discussion 19
3.1 Compressive strength 19
3.2 Single fiber pullout tests 19
3.2.1 Pullout behavior of Bundled fibers 19
3.2.2 Pullout behavior of commercial fibers 22
3.2.3 Comparison between bundled and commercial fibers 22
3.3 Direct tensile tests 23
3.3.1 Tensile behavior of UHPC with different types of steel fibers 23
3.3.2 Influence of fiber parameters on fiber efficiency and fiber utilization 26
3.3.3 Long term tensile behavior of UHPC 30
Chapter 4: Conclusions and Recommendations 36
References 38
Appendix 40

List of Figures

Fig. 1. Fibers with different geometries (from left to right: B2, B3, B4, B5, Straight, Striated, Wavy, Hooked and Twisted) 12
Fig. 2. Test setups for different tests. 14
Fig. 3. Procedure to determine the degree of slip hardening for steel fibers (IP: Intersection point). 16
Fig. 4. Example of the analytical procedure for tensile specimens. (*Note*: (a) corresponds to study for objective 2 while (b) and (c) corresponds to the study for objective 3) 17
Fig. 5. Illustration of calculation procedure of energy values. 17
Fig. 6. Compressive strength of specimens with different types of fibers. 19
Fig. 7. Pullout load, fiber stress and shear stress versus slip curves for bundled fibers. 20
Fig. 8. Pullout response of straight and bundled fiber. 21
Fig. 9. Single fiber pullout behavior of different commercial fibers. 22
Fig. 10. Comparison of degree of slip hardening between various fibers. 23
Fig. 11. Tensile behavior of UHPC with different types of steel fibers 25
Fig. 12. Relationship between softening energy and total fracture energy. 26
Fig. 13. Effect of fiber volume fraction on (a) Relative fiber efficiency factor and (b) Relative fiber utilization factor. 26
Fig. 14. Effect of aspect ratio on (a) fiber efficiency factor and (b) fiber utilization factor. 27
Fig. 15. Effect of surface texture of fiber on (a) fiber efficiency factor and (b) fiber utilization factor. 28
Fig. 16. Effect of fiber geometry on (a) fiber efficiency factor and (b) fiber utilization factor. 29
Fig. 17. Effect of fiber tensile strength on (a) fiber efficiency factor and (b) fiber utilization factor. 29
Fig. 18. Individual curves and average bi-linear model for different series tested at age of 13.5 years. 30
Fig. 19. Comparison of bi-linear models for series tested at 28 days and 13.5 years. 31
Fig. 20. Comparison of elastic parameters for specimens tested at different ages. 32
Fig. 21. Comparison of post cracking parameters for specimens tested at different ages. 32
Fig. 22. Average fiber stress and Equivalent bond for specimens tested at different ages. 33
Fig. 23. Strain for specimens tested at different ages 34
Fig. 24. Energy absorption capacity for specimens at different ages. 34
Fig. 25. Crack spacing for specimens at different ages. 35
Fig. 26. Softening energy for specimens tested at different ages. 35

List of Tables

Table 1. Oxide Composition of Type II Portland cement. 12
Table 2. Properties of steel fibers used as a part of this research. 12
Table 3. Mix proportion of UHPC (by weight) 13
Table 4. Mix proportions by weight [3] 13
Table A-1. Summary of Pullout parameters of bundled fibers. 40
Table A-2. Summary of Pullout parameters of commercial fibers. 40
Table A-3. Summary of tensile parameters of UHPC and corresponding fiber efficiency and fiber utilization factors. 41
Table A-4. Summary of long term tensile properties of UHPC. 42

List of Key Terms

Abbreviation	Definition
ASCE	American Society of Civil Engineers
DOT	Department of Transportation
UHPC	Ultra-High Performance Concrete
US	United States of America
UTC	University Transportation Centers
TIDC	Transportation Infrastructure Durability Center
RH	Relative Humidity
ASTM	American Society for Testing and Materials
l_e	Embedment length
l_f/d_f	Aspect ratio of fiber
l_g	Gauge length
σ_t	Tensile strength of fiber
σ_f	Tensile stress in fiber
σ_{cc}	Fictious Cracking stress of composite
σ_{pc}	Composite tensile strength
$\sigma_{fpc,avg}$	Maximum fiber stress at σ_{pc}
P	Pullout load
S	Slip
IP	Intersection Point
$\tau(s)$	Shear stress
E_{cc}	Elastic modulus
E_{hc}	Strain hardening modulus
E_{pc}	Unloading modulus
τ_{av}	Average bond strength
W_p	Pullout Energy
ε_{cc}	Fictious cracking strain
ε_{pc}	Strain capacity
ε_{soft}	Softening strain
ε_{res}	Residual strain
g_e	Elastic energy
g	Energy absorption capacity
G_f	Fracture energy
$G_{f,b}$	Softening energy
N_f	Number of fibers in cracking plane
e_f	Fiber efficiency factor
u_f	Fiber utilization factor
$\lambda\tau_{eq}$	Equivalent bond
S_{cr}	Crack spacing
$V_f \times l_f/d_f$	Fiber reinforcing index

Abstract

The research performed under this project aims to promote fiber efficiency in Ultra-high performance concrete (UHPC). UHPC derives much of its tensile capacity and durability from the efficiency with which fibers bridge cracks and transfer stresses to the matrix. However, quantifying fiber efficiency across different fiber types, geometries, and long-term conditions remains a critical challenge for structural applications. This report consolidates three experimental investigations aimed at advancing the understanding of fiber efficiency in UHPC. Multiple types of steel fibers having different geometry, tensile strength, aspect ratio and surface texture have been tested to study their efficiency in UHPC.

First, single fiber pullout tests for commercial fibers and newly proposed bundled steel fibers were studied through single fiber pullout tests, and a new slip hardening factor was introduced to characterize performance of steel fibers. Second, a comprehensive testing program was conducted with nine different fiber geometries at multiple volume fractions, enabling the development of new fiber efficiency and utilization factors that capture the interaction between fiber geometry, dosage, and matrix. Third, direct tensile tests were performed on UHPC specimens naturally cured for 13.5 years, revealing the role of fibers in maintaining tensile strength and ductility over time.

Together, these studies highlight the mechanisms governing fiber efficiency in UHPC at the material, structural, and time-dependent scales. The findings provide a unified framework for evaluating and optimizing fiber use in UHPC mixtures, contributing to the design of more durable and resource efficient UHPC.

Chapter 1: Introduction and Background

1.1 Project Motivation

The United States continues to face significant challenges due to its aging and increasingly deteriorated infrastructure. The American Society of Civil Engineers (ASCE) assigned a C grade to U.S. infrastructure in 2025. ASCE estimates that addressing infrastructure deficiencies will require $9.1 trillion in investment, with a $3.7 trillion funding gap between current planned investments and what is needed to bring infrastructure to a state of good repair [1] . If unaddressed, these deficiencies could lead to a projected $10 trillion loss in GDP by 2039 [2].

UHPC is increasingly being considered for demanding structural applications due to its superior strength, durability, and crack resistance. A defining feature of UHPC is the incorporation of steel fibers, which provide crack bridging and tensile capacity that conventional concretes cannot achieve [3]. Despite its growing use, the efficiency with which fibers contribute to UHPC performance remains insufficiently understood, particularly in relation to fiber geometry, dosage, long-term behavior, and alternative fiber arrangements. This knowledge gap has limited the development of rational design guidelines and hindered broader implementation of non-proprietary UHPC in infrastructure.

To address these challenges, this project focuses on building a systematic understanding of fiber efficiency in UHPC through experimental investigations at multiple scales. The first component examines various fibers through single fiber pullout tests, introducing a new slip-hardening factor to quantify their anchorage behavior and potential for enhancing post-cracking toughness. The second component explores a broad matrix of multiple fiber geometries at multiple volume fractions, leading to the development of new fiber efficiency and utilization factors that enable quantitative comparisons across fiber types. The third component investigates the long-term tensile performance of UHPC after 13.5 years of natural curing, offering rare insights into the sustained effectiveness of fibers in maintaining strength and ductility over time.

By integrating these investigations, the project seeks to provide a unified framework for evaluating and optimizing fiber use in UHPC. Such an approach is essential for developing cost-effective, durable, and sustainable non-proprietary UHPC mixtures for structural applications. Ultimately, the motivation driving this work is the need to advance both the scientific understanding and the practical application of efficient fiber utilization in UHPC.

1.2 Research, Objectives, and Tasks

The overarching goal of this project is to improve the understanding and application of fiber efficiency in UHPC for infrastructural applications. The research was structured around three core technical objectives and one knowledge transfer objective, each supported by specific tasks.

Objective 1 – Characterize the bond behavior of steel fibers in UHPC.

- Task 1.1: Perform single fiber pullout tests on conventional steel fibers and bundled steel fibers to evaluate bond performance.
- Task 1.2: Develop a slip-hardening factor to assess the performance of fibers.

Objective 2 – Develop efficiency and utilization factors for multiple fiber geometries.

- Task 2.1: Perform tensile and single fiber pullout testing with multiple fibers at multiple volume fractions.
- Task 2.2: Establish new fiber efficiency and utilization factors that capture fiber-matrix interactions.
- Task 2.3: Provide guidance for optimizing fiber selection in UHPC mixtures.

Objective 3 – Evaluate the long-term tensile performance of UHPC.

- Task 3.1: Conduct direct tensile tests on UHPC specimens stored under natural curing conditions for 13.5 years.
- Task 3.2: Assess changes in tensile strength, strain capacity, and post-cracking behavior relative to 28 days performance.

Objective 4 – Knowledge transfer and industry outreach.

- Task 4.1: Involve undergraduate students in laboratory testing and data analysis to foster training and workforce development.
- Task 4.2: Disseminate results through journal publications, conference presentations, and technical reports.
- Task 4.3: Share findings with industry stakeholders and DOT partners to support broader adoption of non-proprietary UHPC.

1.3 Report Overview

This report is organized into four chapters as follows:

- Chapter 1 provides a general introduction, outlining the background, motivation, goal, and objectives of the study.
- Chapter 2 provides information about the materials used, experimental design and testing procedures.
- Chapter 3 presents and analyzes the test results, with in-depth discussions interpreting the findings and their implications.
- Chapter 4 provides the conclusions and a concise summary of the research outcomes.

Chapter 2: Methodology

2.1 Materials, mix design and sample preparation

The materials used in this study to characterize the bond behavior and to develop efficiency and utilization factors for multiple fiber geometries are Type II Portland cement, undensified silica fume (SiO_2 > 90 %), Type C fly ash (CaO > 18%), basalt aggregates, water, superplasticizer (29% solid content) and steel fibers. The oxide composition of the type II Portland cement is given in Table 1. The types and properties of steel fibers used as a part of this research is provided in Table 2. The images of different geometries of fibers are shown in Fig. 1.

Table 1. Oxide Composition of Type II Portland cement.

CaO	SiO_2	Al_2O_3	Fe_2O_3	SO_3	MgO	K_2O
60.6	16.4	3.4	3.3	3.2	2.1	0.7

Table 2. Properties of steel fibers used as a part of this research.

Geometry	Coating	Length (l_f in mm)	Diameter (d_f in mm)	Aspect ratio (l_f/d_f)	Tensile strength (MPa)
Bundled fibers (B2, B3, B4, B5)	Brass	13	0.2*	65	2850*
Striated (STR)	Brass	10	0.2	50	2850
		13	0.2	65	
		20	0.2	100	
Straight (ST)	Brass	13	0.2	65	2850
Hooked (H)	Stainless	30	0.55	55	1345
Straight (ST-S)	Stainless	13	0.2	65	1310
Wavy (W)	Brass	13	0.2	65	2800
Twisted (T)	Brass	20	0.3	67	2900
Twisted (T)	Galvanized	25	0.5	50	1700

* Properties of single wire, not of bundle

Fig. 1. Fibers with different geometries (from left to right: B2, B3, B4, B5, Straight, Striated, Wavy, Hooked and Twisted)

The UHPC mixture was prepared in a Hobart type mixer. First basalt aggregates and silica fume were dry mixed for five minutes at speed one. Fly ash and cement were then added and mixed for five more minutes. Then, water and one-third of superplasticizer were gradually added to the mix, followed by remaining two-thirds of superplasticizer when the mixer was spinning. The speed was then increased to speed two till the mixture turned over. The speed was reduced back to speed one and the mixing continued for five minutes. Steel fibers were then added to the mix and mixed for two more minutes before pouring to ensure uniform dispersion of fibers. For fiber pullout tests, the same mixture was prepared without the fibers. The mix proportion to characterize the bond behavior and to develop efficiency and utilization factors for multiple fiber geometries is based on Table 3. The specimens are identified using the fiber geometry (STR, ST, ST-S, W, H and T) and the fiber length (10, 13, 20,25 and 30). For example, ST-S13 refers to specimen with straight stainless fiber having 13 mm length and H30 refers to specimen with hooked fiber having 30 mm length. In case of bundled fibers, the specimens are identified using the number of bundles, B2 for two bundles, B3 for three bundles and so on.

Table 3. Mix proportion of UHPC (by weight)

Cement	Silica fume	Fly ash	Basalt aggregates	Water	Superplasticizer	Fiber[a]
1	0.2	0.25	1.2	0.25	0.015	1% -3%

a: by volume

Note: Mixture without fibers was prepared for fiber pullout tests

In addition, the long term study conducted in this research is a continuation of previous research in ref. [3] using the same materials and mixing procedure. The details of mix proportion for this particular study are presented in Table 4. Three different fiber types (straight, hooked, and twisted) were used to investigate the tensile behavior of UHPC. Each specimen is identified by U which stands for UHPC, the used fiber geometry (S, H, T) and the fiber volume fraction (2%, 3%). For example, U-S2 denotes UHPC with 2% by volume of straight steel fibers.

Table 4. Mix proportions by weight [3]

Type	UHPC	UHP-FRC
Cement	1.00	1.00
Silica Fume	0.25	0.25
Glass Powder	0.25	0.25
Water	0.19	0.19
Superplasticizer	0.011	0.011
Sand A	0.31	0.28
Sand B	0.72	0.64
Fiber (Vol %)	0.00	3
Fc’ (cube 28 days) MPa	230	250

The prepared mixture was poured into 50 mm cube mold for compressive strength tests, half dog bones shape molds for fiber pullout tests and dog bone molds for tensile strength test. After pouring, the molds with freshly poured mixtures were vibrated for two minutes, then covered by plastic sheet and allowed to set for 24 hours before demolding. The specimens were then cured for 28 days under normal temperature conditions before testing. While the specimens for long term study were stored in the laboratory at around 23 °C and 60% RH for 13.5 years after initial curing inside water tank at 20 °C for 25 days.

2.2 Test Procedure and Analysis

The images of test setups for different tests are shown in Fig. 2.

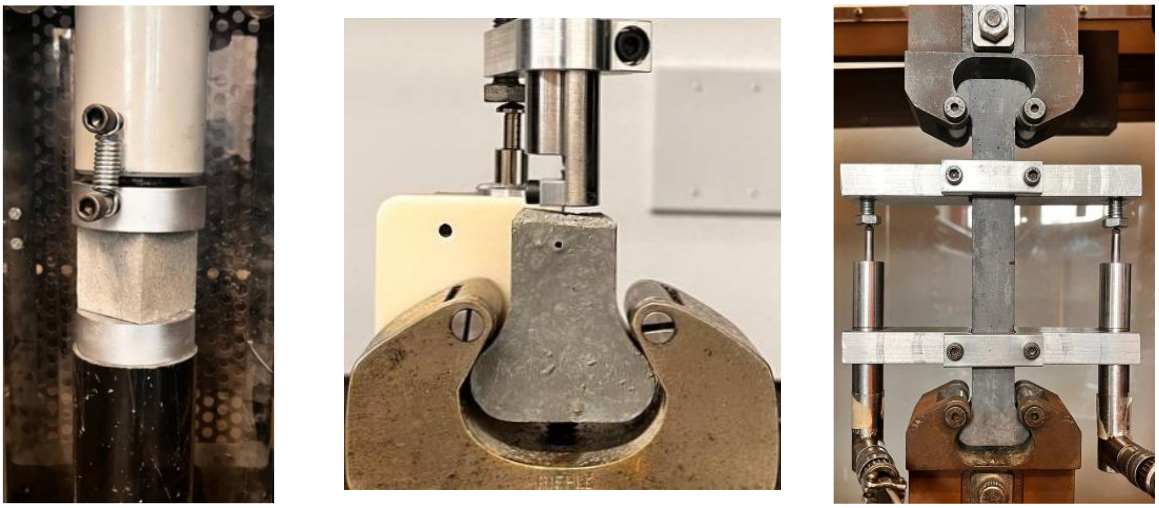

(a) Compression test setup (b) Fiber pullout test setup (c) Tensile test setup

Fig. 2. Test setups for different tests.

At least three specimens were tested for all the tests and the average value with standard deviation is reported. The compressive strength test was done only for samples with 2% fiber volume fraction at the rate of 30,000 lbf/min following ASTM C109/C109M [4]. For fiber pullout tests, two embedment lengths (6.5 mm and half the fiber length) were considered. All the fibers with tensile strength σ_t was embedded both half of the fiber length (l_f/ 2) and 6.5 mm into the UHPC matrix while twisted fibers which embedded only 6.5 mm in the matrix due to fiber failure caused by excessive bond when embedded half the fiber length. All the tests were conducted at the age of 28-30 days of sample preparation.

Fiber pullout tests were conducted at the rate of 1 mm/min. The following parameters were derived from the pullout load (P) versus slip (s) data acquired during testing. Fiber stress (σ_f) which is defined as the tensile stress induced in the fiber is obtained by dividing the pullout load (P) by the

cross-sectional area of the fiber ($A_f = \pi d_f^2/4$) where (d_f) is the diameter of the fiber. Here, A_f represents the cross-sectional area for one fiber. The maximum fiber stress ($\sigma_{f,max}$) is the fiber stress at maximum pullout load (P_{max}) and the slip capacity (s_{max}) refers to the slip at P_{max}. Shear stress, $\tau(s)$is determined by dividing the pullout load at slip S, $P(s)$ by the current bond surface area (contact perimeter with the matrix × ($L_e - s$)), where L_e is the initial embedment length. Average bond strength (τ_{av}) is the shear stress at maximum pullout load. Pullout energy (W_p) is determined by calculating the area under the pullout load-slip curve. All these parameters are calculated using the equations (1), (2), (3), (4) and (5) given below:

$$\sigma_f = \frac{P}{A_f} \text{ in MPa } (\text{N/mm}^2) \tag{1}$$

$$\sigma_{f,max} = \frac{P_{max}}{A_f} \text{ in MPa } (\text{N/mm}^2) \tag{2}$$

$$\tau_{av} = \frac{P_{max}}{Contact\ perimeter \times L_e} \text{ in MPa } (\text{N/mm}^2) \tag{3}$$

$$\tau(s) = \frac{P(s)}{Contact\ perimeter \times (L_e - s)} \text{ in MPa } (\text{N/mm}^2) \tag{4}$$

$$W_p = \int_{s=0}^{s=L_e} P(s)\, ds \text{ in Nmm } (\text{J} \times 10^{-3}) \tag{5}$$

Additionally, a new equation is proposed to quantify the degree of slip hardening for steel fibers. This involves analyzing the pullout load-slip curve by fitting two lines: one for the fully bonded zone and another for the slip hardening zone. The point of intersection (IP) of these lines is identified, and a vertical line is drawn from IP to intersect the pullout load-slip curve at the pullout load (P_{db}) and slip (s_{db}). These values, P_{db} and s_{db} represent the pullout load and slip when the fiber begins to slip after debonding from the matrix. These parameters are then compared with the maximum pullout load (P_{max}) and slip capacity (s_{max}). An illustration is shown in Fig. 3 and the equation to calculate the degree of slip hardening is given by,

$$\text{Degree of slip hardening} = \frac{P_{max} - P_{db}}{P_{max}} \times \frac{s_{max} - s_{db}}{s_{max}} \tag{6}$$

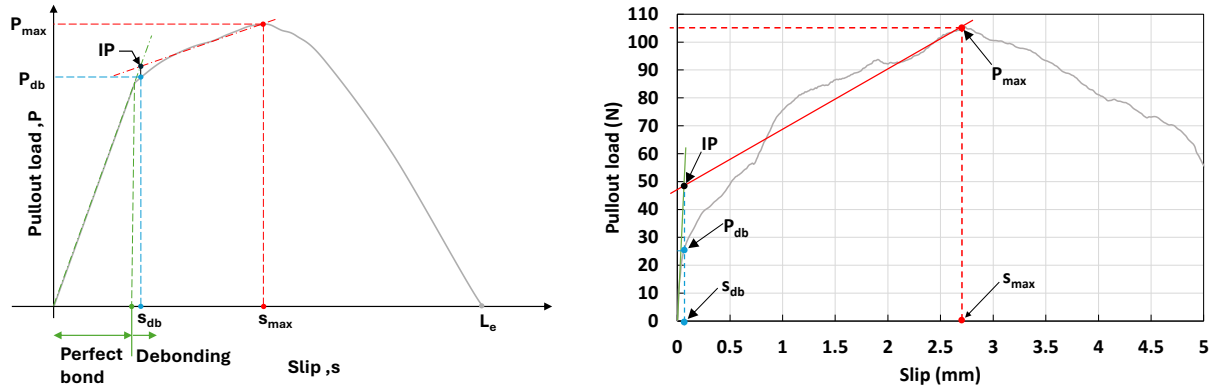

(a) Illustration

(b) B2 at an embedment length of 6.5 mm

Fig. 3. Procedure to determine the degree of slip hardening for steel fibers (IP: Intersection point).

The tensile tests were conducted at a loading rate of 0.6 mm/min. Once the peak tensile strength was reached and the specimen started to enter the softening stage with fibers starting to get pulled out, the samples were unloaded till 1 MPa and reloaded back at the same rate till the complete separation of dog bones.

The test data were analyzed to obtain the parameters $\sigma_{cc}, \varepsilon_{cc}, E_{cc}, \sigma_{pc}, \varepsilon_{pc}, E_{hc}, \varepsilon_{soft}, E_{pc}$ and ε_{res} (see Fig. 4). The parameters $\sigma_{cc}, \varepsilon_{cc}$ and E_{cc} were obtained from the test data during the pre-cracking stage, whereas $\sigma_{pc}, \varepsilon_{pc}, E_{hc}, \varepsilon_{soft}, E_{pc}$ and ε_{res} were obtained from the post-cracking stage. σ_{cc} and ε_{cc} is the stress and strain values at the intersection point of the straight line representing the elastic region and the best fit line of the strain hardening region (Fig. 4b). The strain hardening modulus E_{hc} is defined as the slope of the line joining σ_{cc} and 99% of σ_{pc}. The unloading modulus (E_{pc}) is determined by the line joining the reversal point and the point of interception. The reversal point is the point of minimum stress on the unloading curve while the point of interception is the intersecting point between the unloading and the reloading curve where the composite returns to the stress-strain state prior to unloading. The residual strain (ε_{res}) is taken as the x-intercept as extension of the unloading modulus drawn from 99% of σ_{pc}. An example of the analytical procedure for test specimens for study 2 and 3 is presented in Fig. 4.

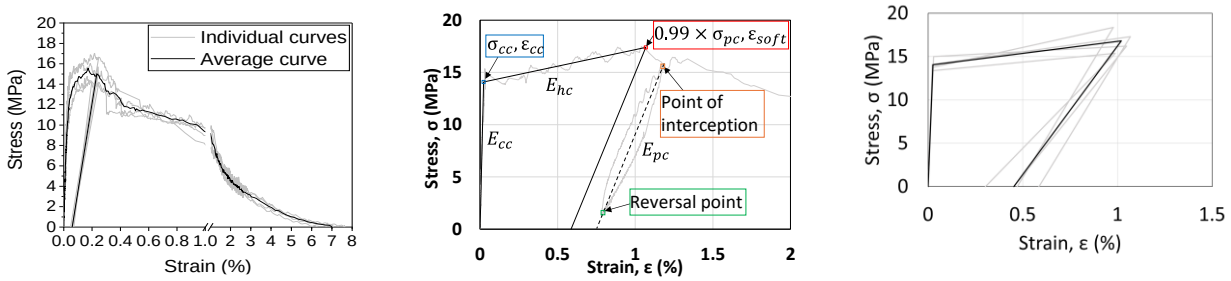

(a) Envelope curve with unloading line (b) Development of bi-linear model (c) Individual and average bi-linear model

Fig. 4. Example of the analytical procedure for tensile specimens. (*Note*: (a) corresponds to study for objective 2 while (b) and (c) corresponds to the study for objective 3)

Additionally to this, the experimental curves are further analyzed using E_{cc}, E_{hc} and E_{pc} to calculate the elastic energy (g_e), energy absorption capacity (g), total fracture energy (G_f) and the fracture energy during softening ($G_{f,b}$) (see Fig. 5).

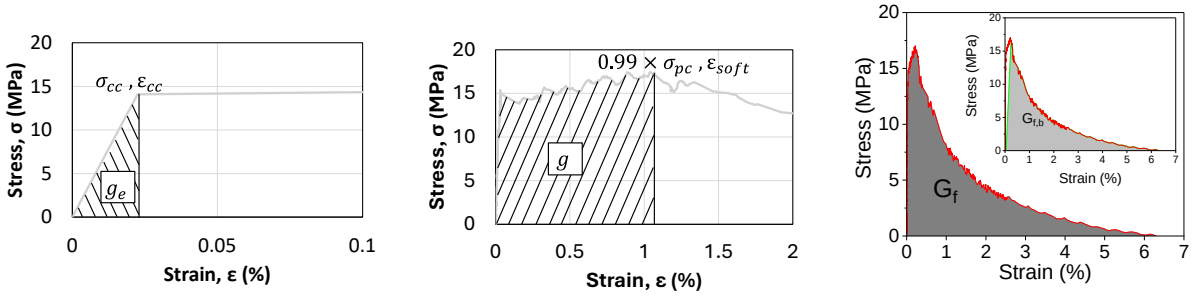

(a) Elastic energy, g_e (b) Energy absorption capacity, g (c) Total fracture energy (G_f) and the fracture energy during softening ($G_{f,b}$)

Fig. 5. Illustration of calculation procedure of energy values.

To determine how efficiently fibers interact with the matrix and the amount of fiber material utilized during the tensile tests, two factors are proposed: fiber efficiency factor and fiber utilization factor. The factor by which the softening energy is less than the product of number of fibers in the cracking plane and the maximum pullout energy of one fiber before pullout is defined as fiber efficiency factor. This factor accounts for all the variables which can influence the performance of fibers in the tensile behavior of UHPC. Hence, the fiber efficiency factor can be expressed as:

$$\text{Fiber efficiency factor } (e_f) = \frac{G_{f,b} \times A_c \times l_g}{100 \times N_f \times W_{p,max}} \tag{7}$$

Here, $G_{f,b}$ is the softening energy, N_f is the number of fibers manually counted from separated dogbones after the tensile test in the cracked surface, A_c is the cross sectional area of the specimen

(25.4 mm × 25.4 mm), l_g is the gauge length (80 mm) and $W_{p,max}$ is the maximum pullout energy of the fiber used in the specimen before pullout.

The extent of utilization of fibers is quantified using fiber utilization factor which is defined as the ratio of maximum tensile stress in the fiber to its tensile strength. Hence, the fiber utilization factor is defined as:

$$\text{Fiber utilization factor } (u_f) = \frac{\sigma_{pc}}{\phi \times V_f \times \sigma_t} \quad (8)$$

Here, σ_{pc} is the composite tensile strength, ϕ is the factor that accounts for the fiber orientation which is used as 0.9 based on ref. [3], [5], V_f is the volume fraction of the fibers and σ_t is the tensile strength of fiber.

Chapter 3: Results and Discussion

3.1 Compressive strength

The compressive strength of specimens with different types of fibers at 2% fiber volume fraction is shown in Fig. 6. The presence of steel fibers prevented explosive failure in all specimens. The compressive strength of specimens ranged from 136 MPa to 156 MPa. Despite some deviation, specimens with low strength fiber such as H30, T25 and ST-S13 (1310-1700 MPa) had compressive strength on lower end of the range (136-142 MPa) whereas the specimens with high strength of fibers such as STR10, STR13, STR20, ST13, W13, and T20 (2800-2900 MPa) had compressive strength towards the higher end of the range (146-156 MPa).

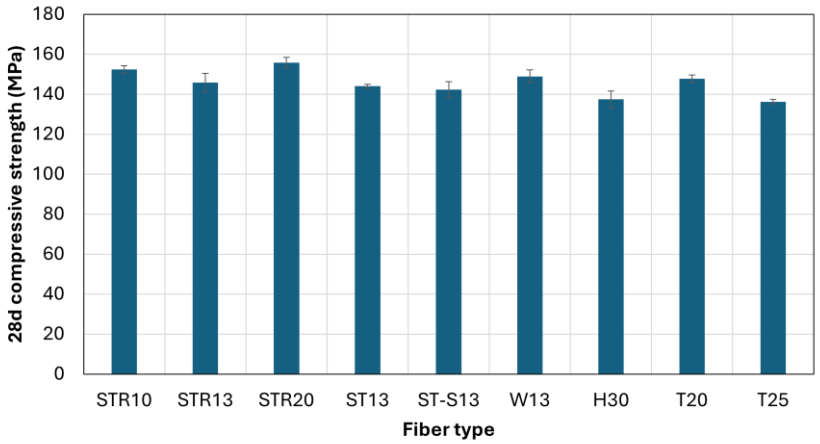

Fig. 6. Compressive strength of specimens with different types of fibers.

3.2 Single fiber pullout tests

3.2.1 Pullout behavior of Bundled fibers

The pullout behavior of the bundled fibers is illustrated in Fig. 7 and the summary of pullout parameters is provided in Appendix (Table A-1) [6]. The presented curve is the average curve of at least four curves. As anticipated, both pullout load and fiber stress increase with longer embedment lengths. Additionally, fibers with a greater number of bundles exhibit higher pullout loads. This is attributed to the increased surface area of fibers with more bundles, which enhances the contact area with the matrix. This larger contact area improves adhesive and frictional forces, resulting in a higher pullout load. Moreover, the debonding process for bundled fibers becomes more gradual as the number of fibers in a bundle increases. This gradual progression enhances pullout resistance and subsequently increases the pullout load. Typically, fibers without slip hardening behavior exhibit a sharp increase in pullout load followed by a decline due to reduced embedment length and diminished bond strength [7]. In such cases, the maximum pullout load is achieved at a small fraction of the embedment length.

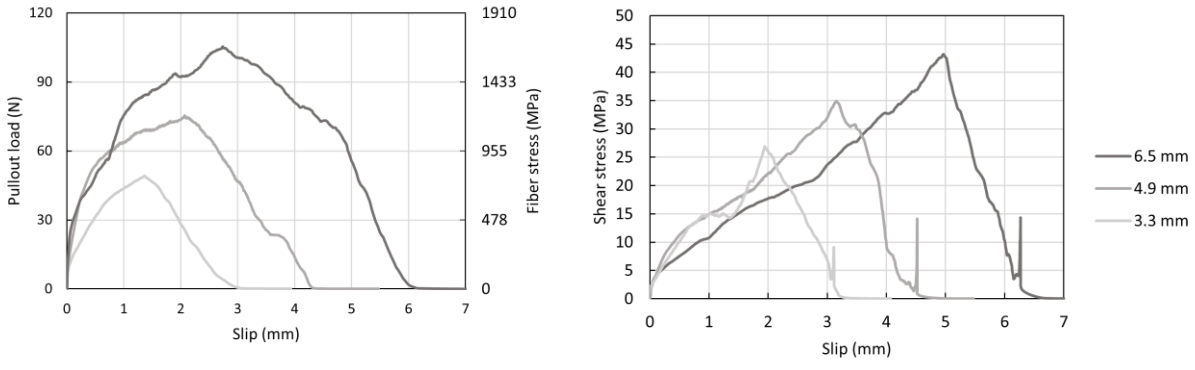

(a) B2

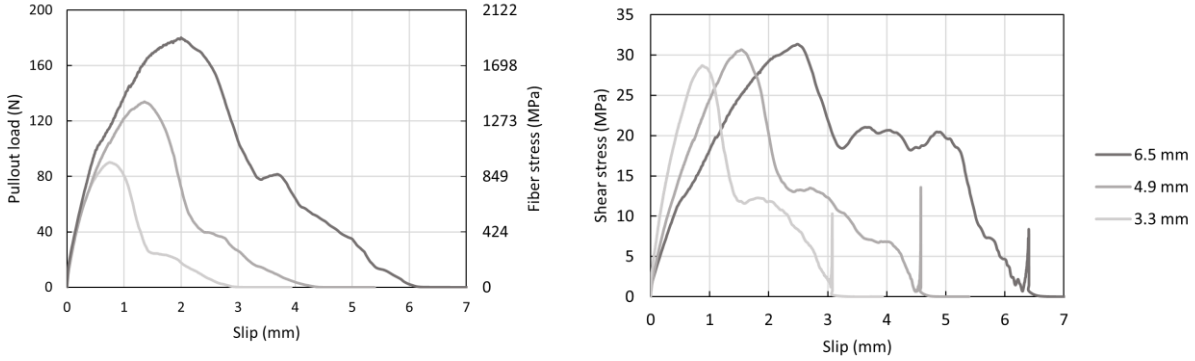

(b) B3

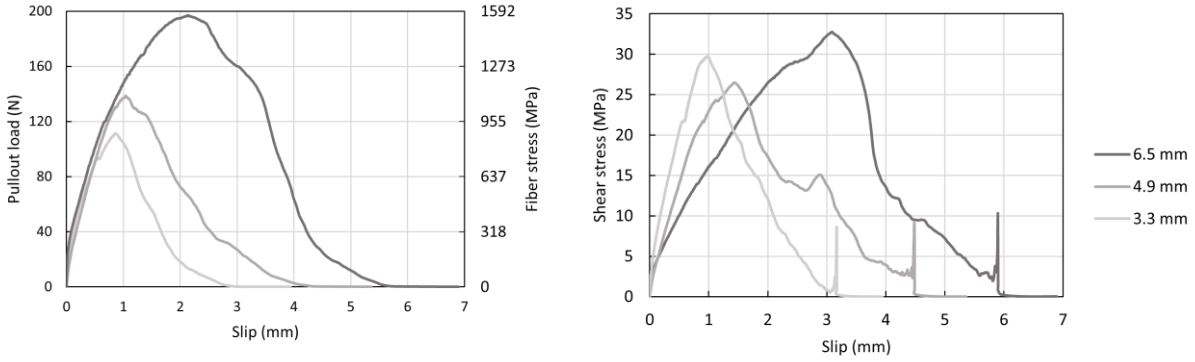

(c) B4

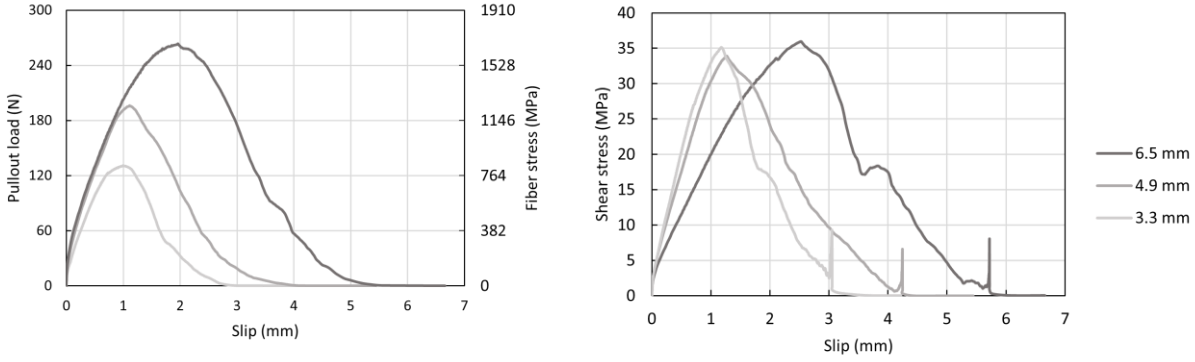

(d) B5

Fig. 7. Pullout load, fiber stress and shear stress versus slip curves for bundled fibers.

In contrast, the bundled fibers demonstrated an increase in pullout load extending up to one-third of the embedment length, and in some cases, nearly half of the embedment length - a slip capacity that is uncommon in a UHPC matrix. This behavior can be attributed to the straightening effect of the twisted bundled fibers during pullout (Fig. 8b). This straightening or untwisting during pullout induces a torque moment which increases the fiber surface pressure of the embedded bundle. As a result, the frictional bond along the embedded bundle increases and thus provides additional anchorage with the matrix. In comparison Fig. 8a shows the pullout mechanism for straight fibers embedded in UHPC. When fibers are pulled out of UHPC matrix, abraded particles or hydration products from the concrete can get trapped between the fiber and the surrounding concrete. This creates pressure on the fiber's surface, increasing friction and enhancing the bond between the fiber and concrete. This effect can lead to slip hardening behavior of even straight fibers in highly dense UHPC [8]. Such slip hardening behavior is advantageous for achieving tensile strain hardening properties in the composite.

Fibers with longer embedment lengths showed higher maximum pullout loads, fiber stress, slip capacity and pullout energies. This increase in pullout parameters was due to the enhanced surface area. The average bond strength remained consistent across different embedment lengths, as the increased pullout load was offset by the longer embedment length. The maximum pullout load, average bond strength and pullout energy increased despite a decrease in slip capacity when the number of bundles increased from B2 to B5 while the maximum fiber stress remained consistent as the increased pullout load was balanced by the larger cross-sectional area.

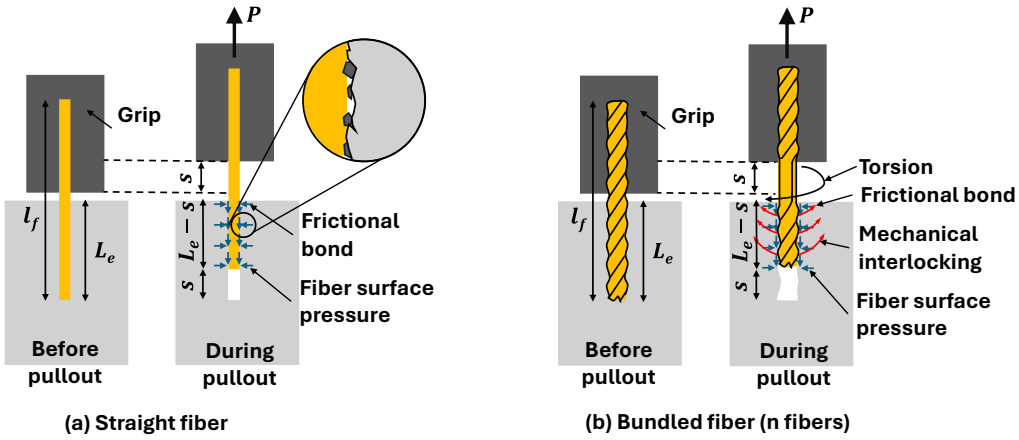

Fig. 8. Pullout response of straight and bundled fiber.

3.2.2 Pullout behavior of commercial fibers

Single fiber pullout behavior of all the fibers used in this study is shown in Fig. 9. The summary of pullout parameters for commercial fibers is provided in Appendix (Table A-2). As expected, fibers with mechanical anchorage (H30, T20, T25) exhibited the highest pullout loads (153–304 N) and pullout energies (455–1108 N-mm). The STR series without anchorage showed lower loads (36–63 N) and energies (62–156 N-mm), though values increased consistently with embedment length due to larger bonding surface. Other fibers (ST13, ST-S13, W13) remained below 35 N in pullout load and 150 N-mm in pullout energy.

In terms of maximum fiber stress, fibers with mechanical anchorage mobilized 1067–2168 MPa, and the fiber utilization was higher (75–91%), indicating that mechanical anchorage effectively mobilizes the tensile capacity. For the STR series of fibers, σ_{max} increased from 1155 to 1995 MPa as the embedment length increased from 5 to 10 mm, corresponding to an increase in fiber utilization from 41% to 70%. Other fibers achieved stresses ranging from 815 to 1087 MPa and fiber utilization from 35 to 62%, with the higher utilization (62%) observed for fiber of lower tensile strength, allowing a greater fraction of their capacity to be mobilized. These findings are consistent with the literature [8-12]. Overall, these results indicate that fiber utilization in single-fiber pullout test is maximized by tailoring the fiber stress to strength of the fibers: (i) stress can be enhanced through mechanical anchorage and higher embedment length, and (ii) by selecting fibers whose tensile strength is balanced with the achievable pullout stress.

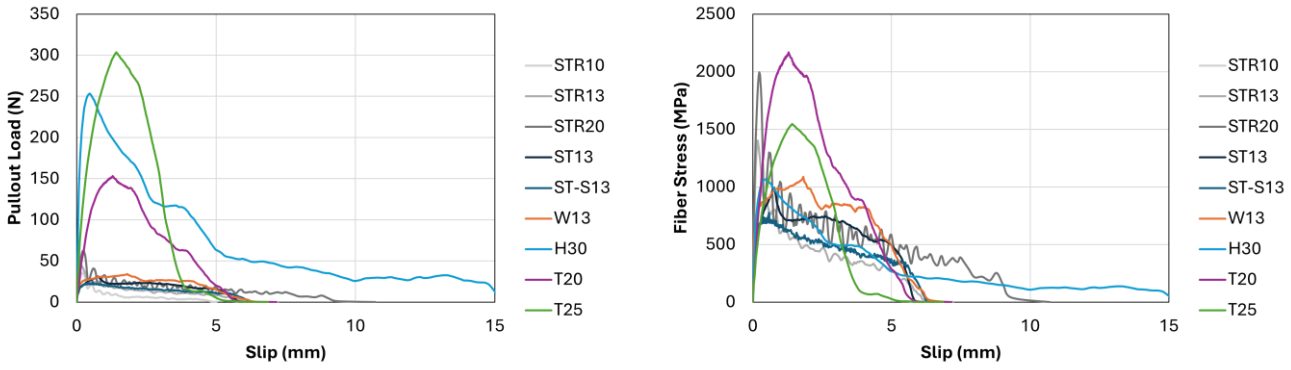

(a) Pullout load - slip behavior (b) Fiber stress – slip behavior

Fig. 9. Single fiber pullout behavior of different commercial fibers.

3.2.3 Comparison between bundled and commercial fibers

The degree of slip hardening was computed to draw comparison between bundled fibers and commercial fibers by using the procedure described in section 2.2 Test Procedure and Analysis.

Here, the parameters P_{db} and S_{db} were determined from the average pullout load-slip curve for each type of fiber. The comparison between different types of fiber in terms of degree of slip hardening is shown in Fig. 10. The bundled fibers exhibited a larger degree of slip hardening with values ranging from 0.72 to 0.78 and outperformed all other types of fibers. Among the others, twisted fibers showed the next best performance with a slip hardening of 0.7, while the remaining fibers had values below 0.55. Hooked fibers which have a mechanical bond with the matrix through bending show the lowest degree of slip hardening of 0.08. This was followed by striated, wavy and straight fibers with the values of 0.15, 0.45 and 0.55. The second closest fiber to the bundled fiber is the twisted fibers with a value of 0.7. Both the twisted and bundled fibers employ a mechanical bonding mechanism through torsion. However, the bundled fibers have been designed to activate an additional straightening effect (see Fig. 8), resulting in a further increase in degree of the slip hardening up to 0.78.

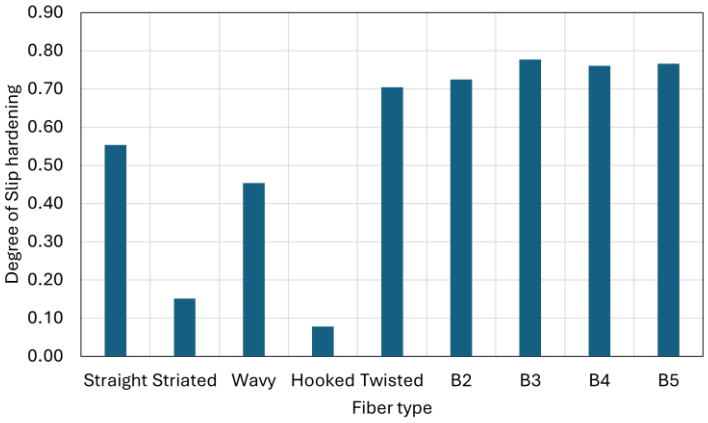

Fig. 10. Comparison of degree of slip hardening between various fibers.

3.3 Direct tensile tests

3.3.1 Tensile behavior of UHPC with different types of steel fibers

The average stress-strain curve from tensile tests for all the specimens at different fiber volume fraction is presented in Fig. 11. The summary of tensile parameters and corresponding factors are given in Appendix (Table A-3).With increasing fiber volume, all the samples show increase in composite tensile strength, fracture energy and softening energy as evident in Fig. 11. On average across all fiber types when the fiber content increased from 1% to 2%, σ_{cc} and σ_{pc} increased by 18% and 30%. However, when the fiber content increased from 2% to 3%, the improvement declined, with σ_{cc} increasing by 14% and σ_{pc} by 17%. This indicates that beyond 2%, while higher fiber content enhances the tensile behavior, the improvement is less pronounced as the fiber

content increases. This is because, although the higher fiber content increases the number of fibers per unit volume, it also leads to group effect, difficulty in dispersion, thereby reducing the overall efficiency of stress transfer and limiting the gains in tensile strength. The samples within the same fiber type (STR series) shows improved tensile behavior with increasing aspect ratio of fibers. When the aspect ratio increased from 50 (STR10) to 65 (STR13), σ_{pc} increased by 24%. On further increase in aspect ratio from 65 (STR13) to 100 (STR20), σ_{pc} increased by 26% indicating that the larger aspect ratio up to 100 is beneficial for enhancing the tensile behavior of UHPC. The fibers with higher aspect ratio have larger bonding area with the matrix which leads to better fiber-matrix bond strength and improved crack bridging, leading to increased tensile strength [14], [15]. When comparing the fibers with same geometry and aspect ratio but different surface texture (STR13, ST13, ST-S13), significant difference was not observed on average in the values of σ_{cc} and σ_{pc}. This shows that the fibers contribution is limited by how much stress can be transferred at the interface rather than its intrinsic tensile strength. Hence, despite the large difference in tensile strength of the fibers, the difference in tensile performance of the composite was not significant. This suggests that the use of very high tensile strength fibers may not always be necessary, as comparable composite strength can be achieved even with lower strength fibers, provided they have similar aspect ratio. Furthermore, among the fibers having different geometries (ST13, W13, H30, T20, T25), the series H30 and T25 show slightly lower strength values than the series ST13, W13and T20. On average across all fiber volume fraction, series H30 showed 8%, 23% and 18% lower σ_{cc} value than ST13, W13 and T20 series. Also, the σ_{pc} values for H30 were 9%, 25% and 20% lower than ST13, W13 and T20 series. Similar trend was observed for T25 series which exhibited 10%, 25% and 20% lower σ_{cc} value and 5%, 22% and 17% lower σ_{pc} value than ST13, W13 and T20 series, respectively. This is most likely due to the difference in aspect ratio of these fibers. The fibers in series ST13, W13 and T20 have relatively higher aspect ratio (65-67), while the series H30 and T25 have fibers with lower aspect ratio (50-55). This results in higher bond surface area per unit cross section of the fiber which leads to higher stress transfer efficiency thus improved tensile behavior. The results indicate that fiber aspect ratio (up to 100) is the most critical parameter for achieving higher tensile strength in UHPC. When fibers have a sufficiently high aspect ratio, they can enhance tensile performance more effectively than fibers with higher intrinsic tensile strength alone provided that enough stress is induced in the fiber.

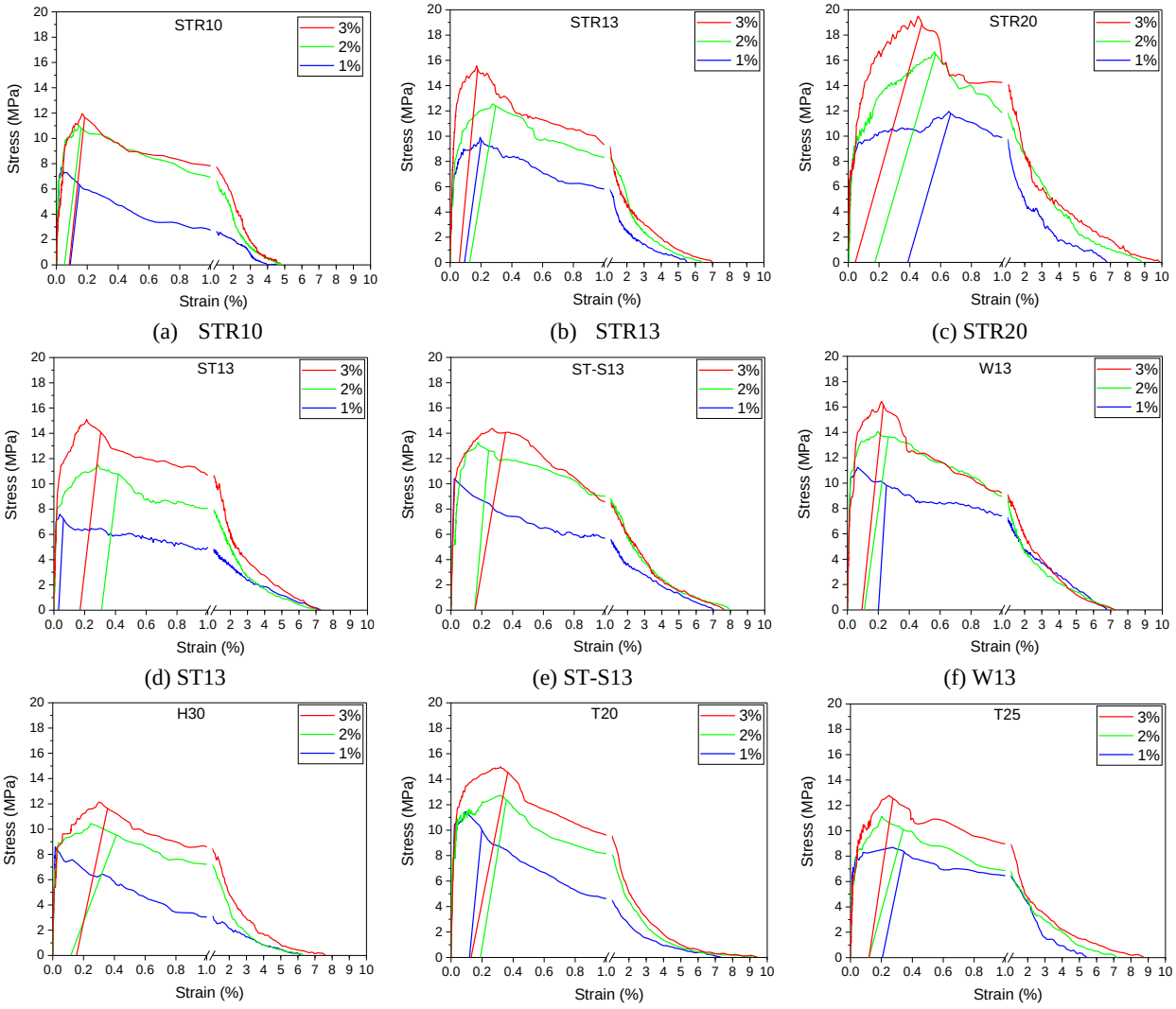

(a) STR10 (b) STR13 (c) STR20

(d) ST13 (e) ST-S13 (f) W13

(g) H30 (h) T20 (i) T25

Fig. 11. Tensile behavior of UHPC with different types of steel fibers

Similar to the other tensile strength parameters, the fibers with higher aspect ratio result in higher fracture energy and subsequently higher softening energy of composite. On average, across all fiber volume fraction, specimens having fibers with aspect ratio of 65-67 show at least 30% lower fracture energy than the those with aspect ratio of 100. Similarly, samples with aspect ratio of 50-55 show more than 40% lower fracture energy than the ones with aspect ratio of 100. In addition, the relationship between total fracture energy and the softening energy is presented in Fig. 12. A trendline is drawn with an equation to predict the softening energy from the total fracture energy. High R square value of over 0.99 indicates a strong correlation in prediction of softening energy.

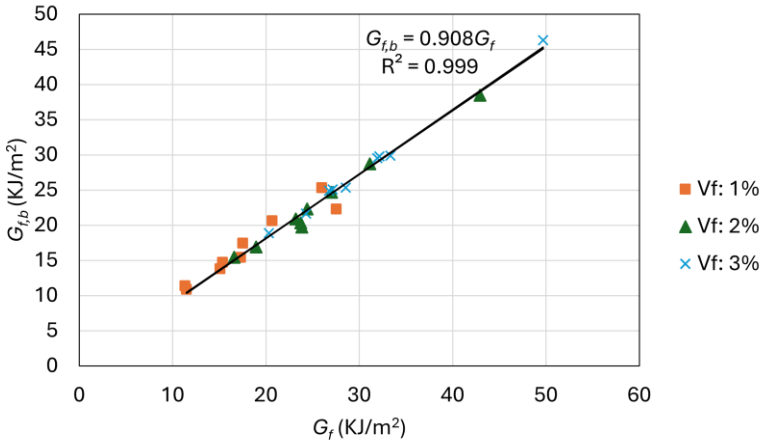

Fig. 12. Relationship between softening energy and total fracture energy.

3.3.2 Influence of fiber parameters on fiber efficiency and fiber utilization

Effect of fiber volume (V_f): The effect fiber volume on e_f and u_f is shown in Fig. 13. To isolate the effect of V_f for each series, the change in e_f and u_f is shown relative to the value at 1% volume fraction. With increasing V_f, both the factors show decreasing trend. In case of e_f, it is most likely due to the increase in group effect of fibers leading to less efficient transfer of stress. Moreover, despite the same casting method, with increase in V_f the fibers have less freedom in aligning with the flow direction, which leads to some random orientation thereby reducing the fiber efficiency. Some deviations are observed, which is because of different mechanisms for different types of fibers leading to range of values for e_f. In case of u_f, the drop is due to the group reduction of bond, which leads to decrease in bond strength resistance per fiber when the number of fibers pulling out from same area increases. This leads to less significant increment in tensile strength in comparison to the fiber volume thereby reducing u_f.

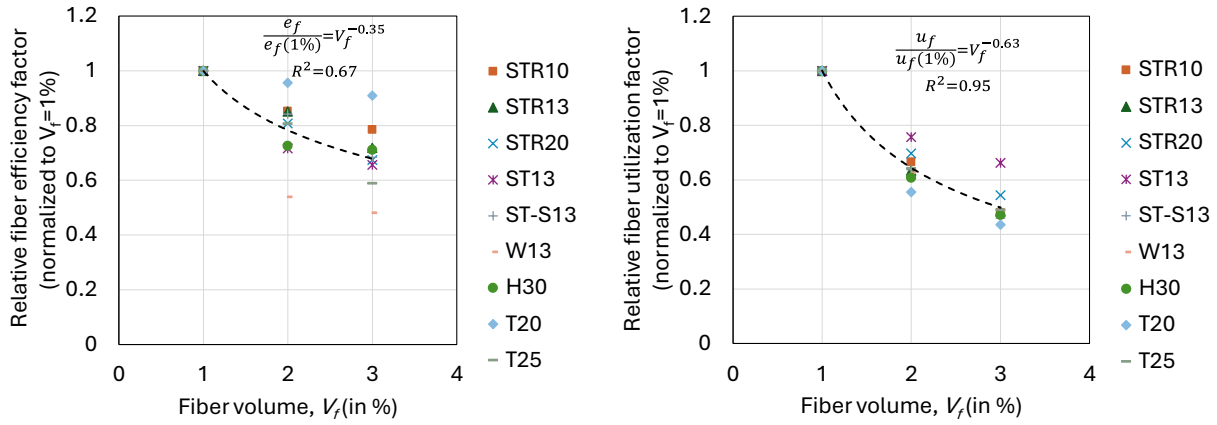

(a) (b)

Fig. 13. Effect of fiber volume fraction on (a) Relative fiber efficiency factor and (b) Relative fiber utilization factor.

Effect of aspect ratio: The effect of aspect ratio of one group of fibers (STR10, STR13 and STR20) on e_f and u_f is shown in Fig. 14. The aspect ratio of fibers did not exhibit a consistent trend in influencing e_f values. This suggests that the efficiency factor is not primarily governed by the aspect ratio but rather how effectively the fiber performs. Consequently, even a fiber with lower aspect ratios can have high efficiency factors when utilized properly by minimizing the orientation and group effects. However, the u_f values showed increasing values with increasing aspect ratio. When the aspect ratio increased from 50 to 100, the specimens exhibited nearly 50% increase in the u_f value. This is because with longer length, fewer fibers are needed to achieve the same reinforcement, and a greater length of each fiber can bridge cracks, improving stress transfer, thus leading to higher u_f values.

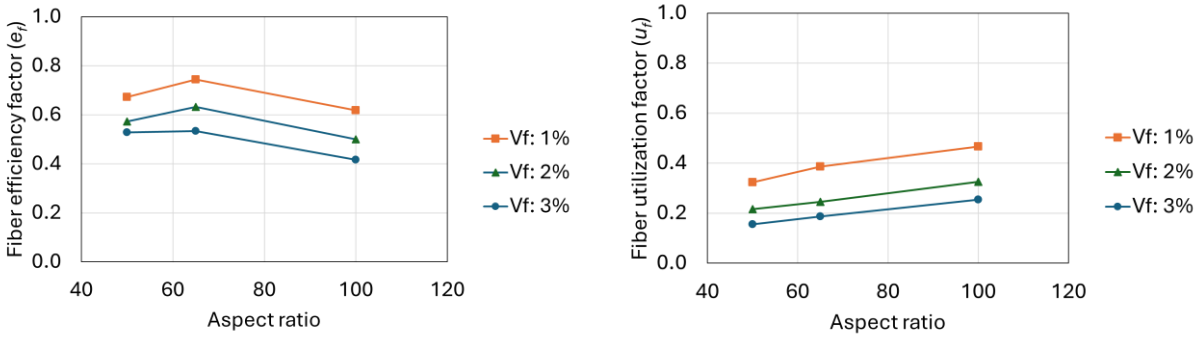

(a) (b)

Fig. 14. Effect of aspect ratio on (a) fiber efficiency factor and (b) fiber utilization factor.

Effect of surface texture: The effect of surface texture is investigated by analyzing three fibers with straight geometry but having different surface textures: striations in the surface (STR13), smooth surface with brass coating (ST13) and smooth surface of stainless steel (ST-S13). The effect of these variations on e_f and u_f values are shown in Fig. 15. Despite the fibers STR13 and ST13 having same tensile strength (2850 MPa), e_f and u_f values for STR13 were higher than that of ST13. Higher e_f values is due to the pullout energy being higher for ST13 fiber than STR13 fiber, which is likely due to the surface damage in straight fibers while pulling out from UHPC matrix causing higher pullout energy despite lower maximum pullout load [13]. This same behavior could not be replicated during the tensile behavior hence the lower efficiency of the ST13 fiber than STR13 fiber. While the higher u_f values are due to the striations present in the surface of STR13 which helps to improve the bonding with the UHPC matrix [16], leading to higher degree of fiber utilization. Furthermore, the fiber ST-S13 despite the lower tensile strength (1310 MPa) shows

higher e_f and u_f values than both STR13 and ST13. This can be attributed to reduced underutilization of fiber ST-S13 than ST13 and STR13 because of its tensile strength being lower and aligning more closely with the actual demand in the matrix allowing it to be more effectively utilized. This keeps the tensile performance of specimens with ST-S13 comparable to that of the ones with STR13 and ST13. Hence the higher e_f and u_f values.

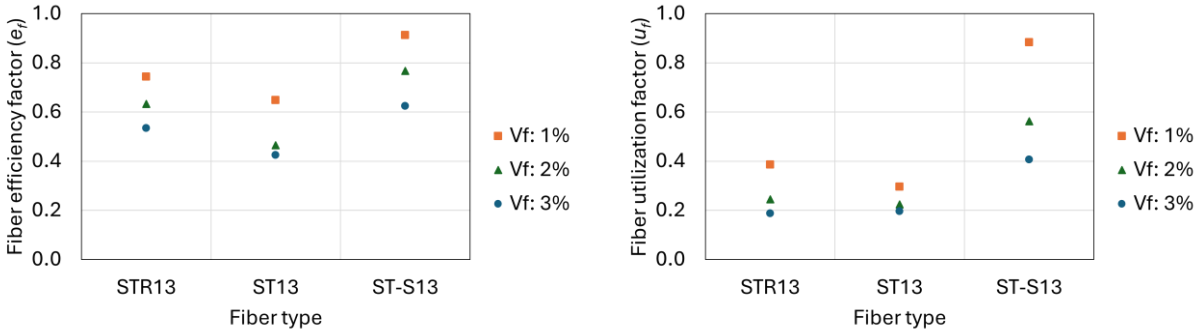

(a) (b)

Fig. 15. Effect of surface texture of fiber on (a) fiber efficiency factor and (b) fiber utilization factor.

Effect of fiber geometry: The effect of five different fiber geometries: Straight (ST13), Hooked (H30), Wavy (W13) and Twisted (T20 and T25) on e_f and u_f values are shown in Fig. 16. The fibers with additional anchorage (H30, T20 and T25) show lower e_f values than ST13 and W13 fibers. This is because the anchorage does not contribute to the improvement of tensile strength as it does for the pullout behavior. For instance, the degree of fiber utilization in these fibers from single fiber pullout tests is at least 75% (79% for H30, 75% for T20 and 91% for T25) which is significantly higher than that of ST13 and W13 (35% for ST13 and 39% for W13). This also results in higher pullout energy and indicates that higher intrinsic tensile strength of fiber can be utilized when additional mechanical anchorage is present in the fiber. However, the tensile behavior of H30, T20 and T25 series does not show improved behavior than that of ST13 and W13 series (see Fig. 11). In fact, only the series T20 has a comparable tensile response, while the series H30 and T25 have lower tensile response than series ST13 and W13. This explains that the improved pullout response due to anchorage does not necessarily translate to the tensile behavior at specimen level. Hence, the lower e_f values for H30, T20 and T25 series than ST13 and W13 series. On the other hand, series H30 and T25 show higher u_f values than other series. This can be attributed to the lower tensile strength of H30 (1345 MPa) and T25 fibers (1700 MPa) than ST13 (2850 MPa), W13 (2800 MPa) and T20 fibers (2900 MPa). Although ST13, W13, and T20 fibers possess higher tensile strengths and demonstrate better tensile responses, the magnitude of improvement in tensile

strength is not proportional to the increase in their tensile properties when compared to H30 and T25. This indicates significant underutilization of fiber strength in ST13, W13, and T20, leading to lower u_f values for these series.

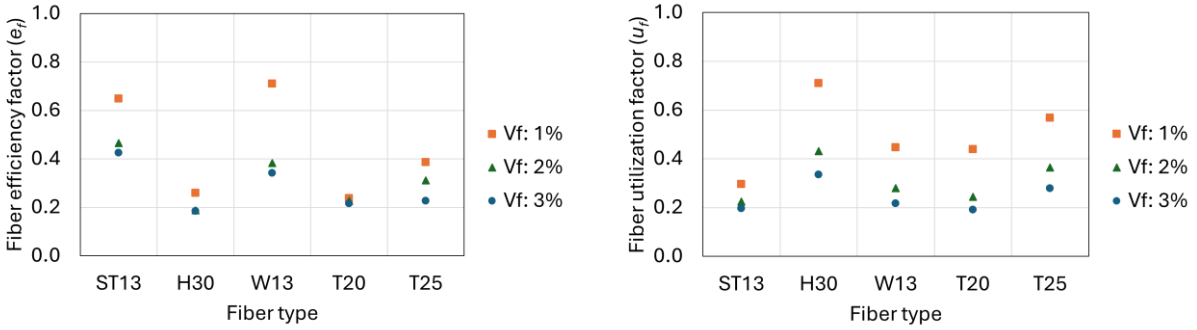

(a) (b)

Fig. 16. Effect of fiber geometry on (a) fiber efficiency factor and (b) fiber utilization factor.

Effect of fiber tensile strength: The effect of range of tensile strength of fibers on e_f and u_f values are shown in Fig. 17. The tensile strength of fibers did not show a consistent influence on e_f values, indicating that fiber efficiency depends more on how effectively the fibers engage with the matrix to reach their maximum potential at the specimen level, rather than on their intrinsic tensile strength. However, the u_f values showed decreasing trend with increase in tensile strength of fibers, indicating that fibers with higher tensile strength were significantly underutilized at the specimen level, likely due to limitation in bonding and the group effect of fibers. This suggests that achieving higher fiber utilization requires careful consideration of multiple factors, including the matrix strength and its ability to mobilize the fibers tensile capacity. Therefore, it may be more effective to use fibers with moderate tensile strength that can be more engaged by the matrix, rather than employing high-strength fibers whose strength goes largely unutilized.

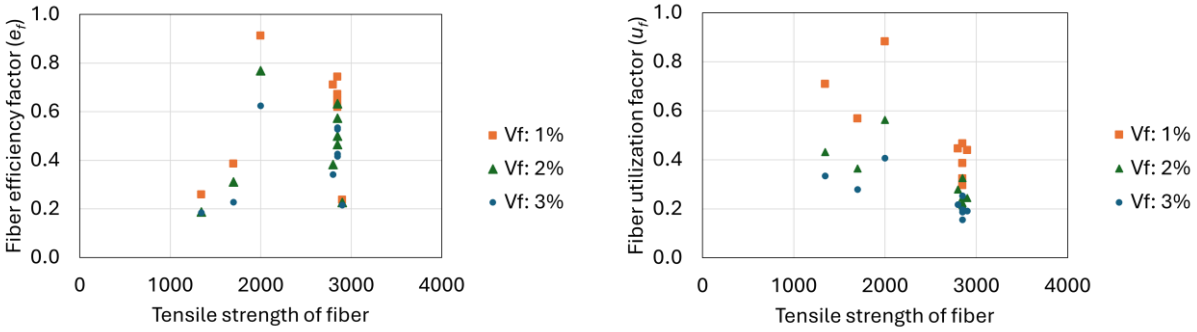

(a) (b)

Fig. 17. Effect of fiber tensile strength on (a) fiber efficiency factor and (b) fiber utilization factor.

3.3.3 Long term tensile behavior of UHPC

Individual stress-strain curves of all tested specimens along with average bi-linear model following procedure explained in section 2.2 Test Procedure and Analysisare illustrated in Fig. 18. Furthermore, the comparison of average bi-linear models between series tested at 28 days and 13.5 years is shown in Fig. 19. The summary of tensile parameters after 28 days of curing and 13.5 years of curing is provided in Appendix (Table A-4).

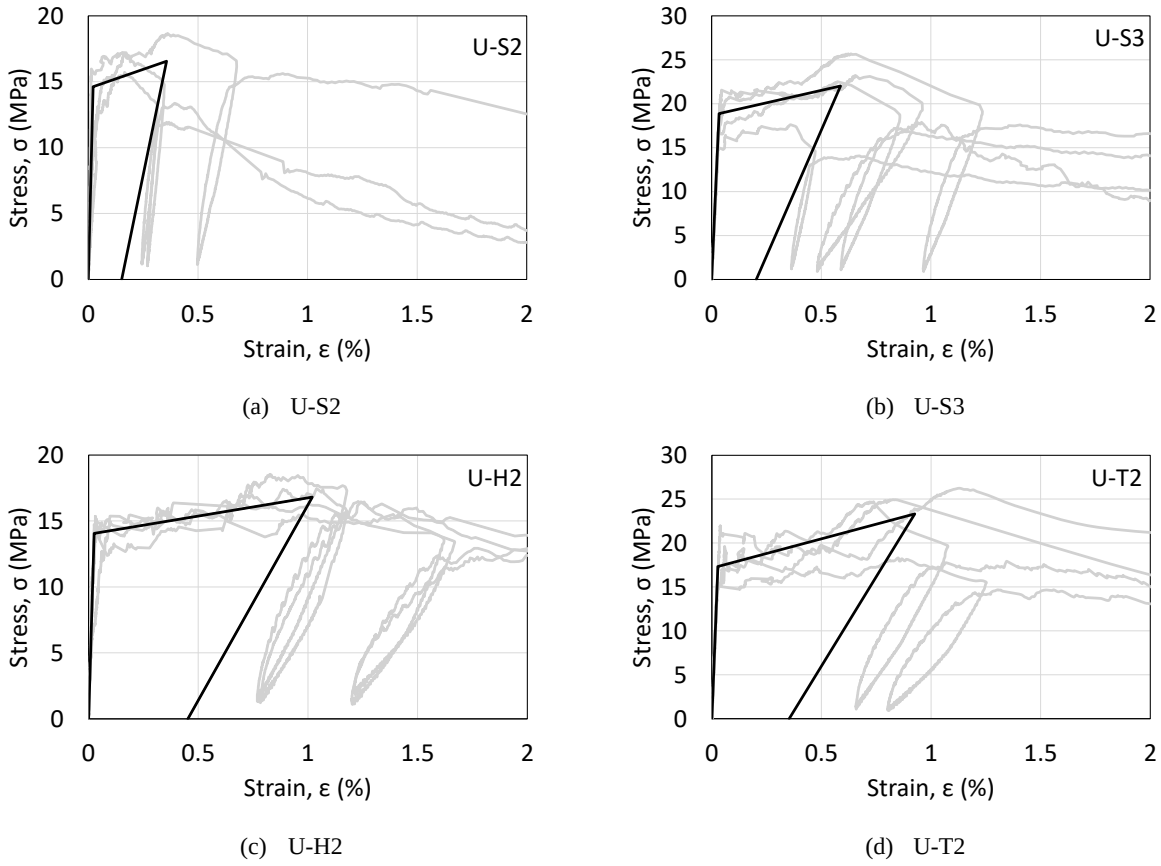

(a) U-S2 (b) U-S3

(c) U-H2 (d) U-T2

Fig. 18. Individual curves and average bi-linear model for different series tested at age of 13.5 years.

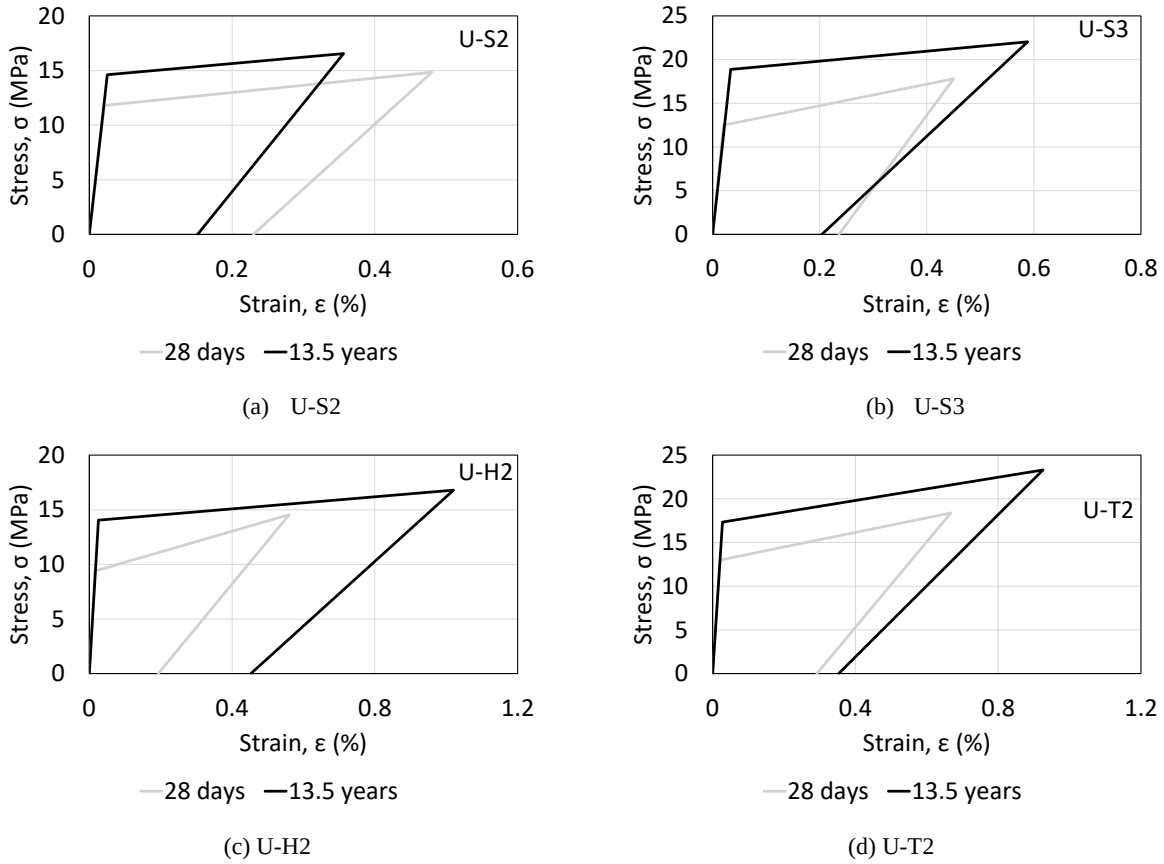

(a) U-S2 (b) U-S3

(c) U-H2 (d) U-T2

Fig. 19. Comparison of bi-linear models for series tested at 28 days and 13.5 years.

The tensile behavior after long term curing is compared in terms of three regions: Elastic region, Strain hardening region and Strain softening region.

Elastic region: Fig. 20 shows the comparison between σ_{cc} and g_e for the 28 days and 13.5 years series, respectively. As expected, the values of σ_{cc} and g_e increased as the specimens aged due to further matrix densification. For example, U-S2, U-H2, U-T2, and U-S3 showed an increase in σ_{cc} by 24%, 49%, 33% and 51%, respectively. Similar to the findings in [3], σ_{cc} showed dependency on fiber volume. Additionally, a higher σ_{cc} increase was observed with modified fiber geometry (U-H2 and U-T2) in comparison to U-S2. The increase in σ_{cc} translated to the increase of g_e as well (Fig. 20b). The series U-S2, U-S3, U-H2 and U-T2 exhibited 47%, 159%, 144% and 76% increment in g_e values after 13.5 years. Due to the marginal increase in strain (ε_{cc}) values from 28 days to 13.5 years the increase in g_e is even higher than that of σ_{cc}.

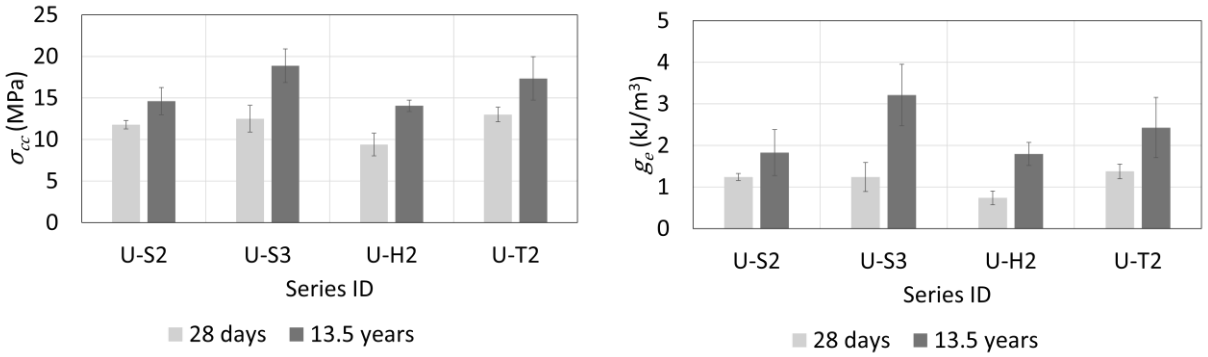

(a) σ_{cc}

(b) Elastic energy, g_e

Fig. 20. Comparison of elastic parameters for specimens tested at different ages.

Strain hardening region: Fig. 21 shows the comparison between the composite tensile strength (σ_{pc}) and the corresponding tensile strain (ε_{pc}) for the series tested at different ages. All series show an increase in σ_{pc} overtime, for example U-S2, U-S3, U-H2 and U-T2 show an increase of 12%, 25%, 16% and 27%, respectively. This confirms that further matrix densification has enhanced the fiber – matrix bond over time and that the limited bond increase did not lead to undesirable fiber ruptures. In comparison to σ_{pc}, ε_{pc} shows an irregular trend for the UHPC with straight fibers, e.g. U-S2 shows almost 16% decrease whereas U-S3 shows nearly 24% increase in ε_{pc} after 13.5 years. Similar irregular tendency was observed in previous studies with ECC [16-18]. However, for both series with modified fiber geometry (U-H2, U-T2) a significant increase in ε_{pc} by 68% and 55% was obtained, respectively. Such high increase over 28 days specimens highlights the significant impact of enhanced fiber matrix bond on the composite behavior of UHPC with H or T fibers.

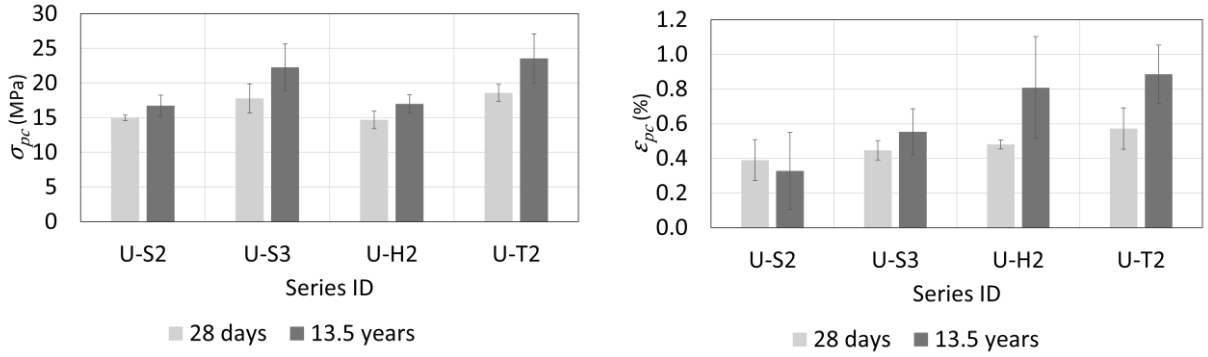

(a) Composite tensile strength, σ_{pc}

(b) Strain at composite tensile strength, ε_{pc}

Fig. 21. Comparison of post cracking parameters for specimens tested at different ages.

The assessments were also made based upon the fiber stress at σ_{pc} ($\sigma_{fpc,avg}$) [3], which is the measure of stress induced in the fiber, and the equivalent bond ($\lambda\tau_{eq}$) [20]. Both of which are determined by equations (9) and (10):

$$\sigma_{fpc,avg} = \frac{\sigma_{pc}}{\Phi \times V_f} \tag{9}$$

$$\lambda\tau_{eq} = \frac{\sigma_{pc}}{V_f \times (\frac{l_f}{d_f})} \tag{10}$$

, where Φ is the fiber orientation factor taken as 0.9 following [3]. Fig. 22 compares $\sigma_{fpc,avg}$ and $\lambda\tau_{eq}$ between the series at 28 days and 13.5 years. As the specimens age, $\sigma_{fpc,avg}$ and $\lambda\tau_{eq}$ increase since these parameters are dependent on the composite tensile strength, indicating higher stress are induced in fibers overtime. As σ_{pc} is the only variable, quantitatively they have the same increment as σ_{pc}. Comparing the different series to each other, it can be seen that increase in fiber volume (V_f) and increase in fiber reinforcing index ($V_f \times l_f/d_f$) lead to decrease in $\sigma_{fpc,avg}$ and $\lambda\tau_{eq}$ (as seen for U-S2, U-S3 and U-H2) unless σ_{pc} is relatively high (as seen for U-T2).

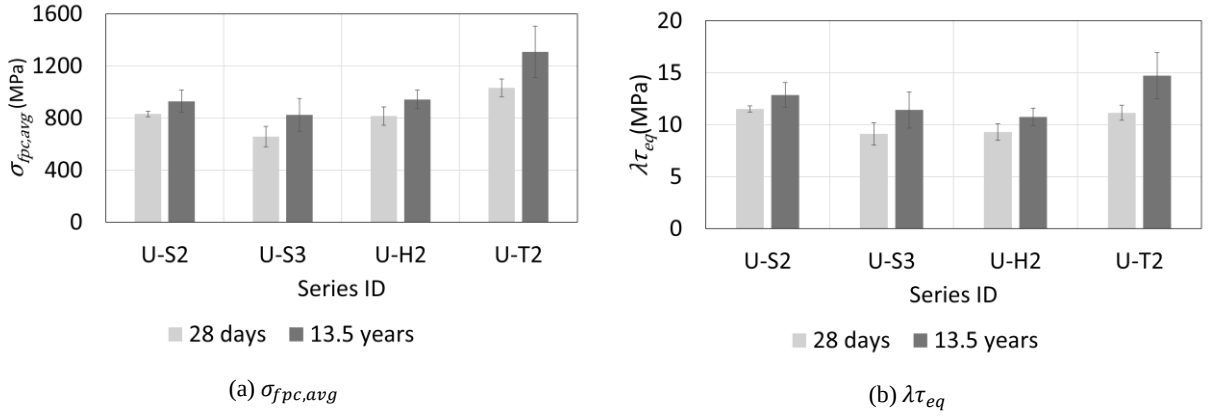

(a) $\sigma_{fpc,avg}$ (b) $\lambda\tau_{eq}$

Fig. 22. Average fiber stress and Equivalent bond for specimens tested at different ages.

Fig. 23 illustrates the comparison of softening strain (ε_{soft}) and residual strain (ε_{res}) for specimens tested at different ages. In the current study, ε_{soft} is taken as the strain at 99% of σ_{pc}, which is presumed as the onset of softening. The trend for ε_{soft} is similar to ε_{pc}. U-S2 showed 25% decrease in ε_{soft} while all other series showed an increase in ε_{soft}, that includes +21%, +83%, and +39% for U-S3, U-H2 and U-T2 in comparison to 28 days.

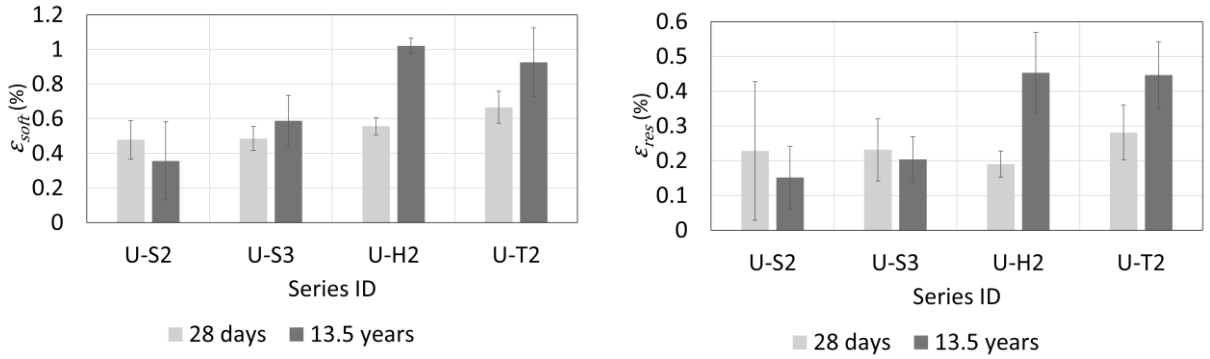

(a) Softening strain, ε_{soft}

(b) Residual strain, ε_{res}

Fig. 23. Strain for specimens tested at different ages

Energy absorption capacity (g), which is the area under the tensile stress-strain curve up to $0.99\times\sigma_{pc}$, is shown in Fig. 24 for different series. The value of g for all series except U-S2 increased with increase in specimen age. U-S2 showed a drop from 67 kJ/m^3 to 38.7 kJ/m^3 due to the drop in strain capacity. Other than this, the values for g increased from 80 kJ/m^3 to 119.2 kJ/m^3, 73.5 kJ/m^3 to 131.3 kJ/m^3 and 112.8 kJ/m^3 to 175.5 kJ/m^3 for U-S3, U-H2 and U-T2, respectively. All the long term series except U-S2 fulfill the performance level 4 of high energy absorbent concrete ($g \geq 50$ kJ/m^3 as defined in [3]) by exceeding the recommended value by a factor of more than two, even three in some case.

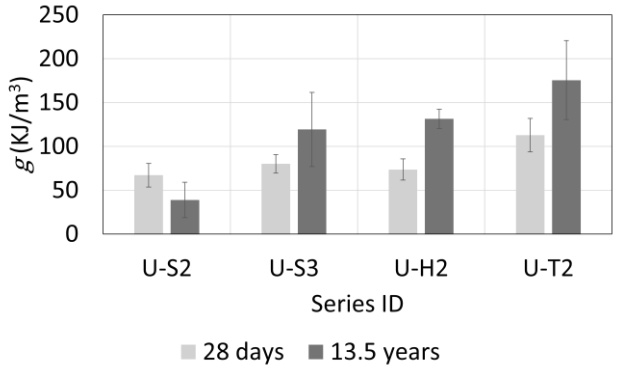

Fig. 24. Energy absorption capacity for specimens at different ages.

Fig. 25 shows crack spacing (S_{cr}) values of all series over time. For all series, S_{cr} decreased for specimens tested at 13.5 years in comparison to at 28 days, e.g. from 4.6 mm to 3.6 mm for U-S2, 3.2 mm to 2.8 mm for U-S3, 5.8 mm to 3.7 mm for U-H2 and 2.4 mm to 2.1 mm for U-T2. This suggests an increase in fiber – matrix bond over time, resulting in a more efficient fiber – matrix load transfer leading to the development of denser multiple cracking and thus a more pronounced

strain hardening. Furthermore, residual crack opening (δ_{pc}) was calculated using parameters $\varepsilon_{soft}, \sigma_{pc}, E_{pc}$ and S_{cr} following equation (11), [3]**:**

$$\delta_{pc} = (\varepsilon_{soft} - \frac{0.99\sigma_{pc}}{E_{pc}}) \times S_{cr} \quad (11)$$

, where the first term is the residual strain ($\varepsilon_{res} = \varepsilon_{soft} - \frac{0.99\sigma_{pc}}{E_{pc}}$) (see Fig. 23b). The value of δ_{pc} ranges from 5 to 16 μm for the specimens. The value decreased for U-S2 from 10.6 μm to 5.5 μm and for U-S3 from 7.5 μm to 5.7 μm, while δ_{pc} increased for U-H2 from 11.2 to 16.7 μm and also marginally increased for U-T2 from 8.9 μm to 9.4 μm.

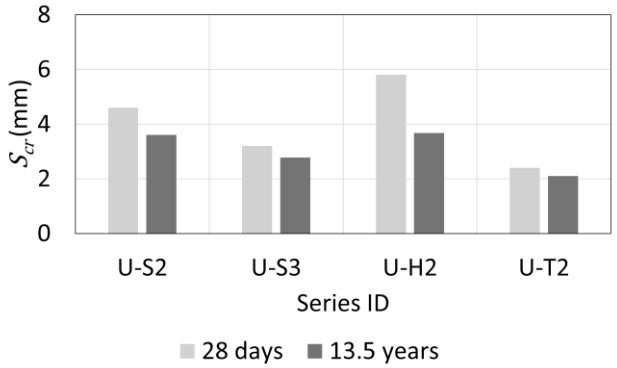

Fig. 25. Crack spacing for specimens at different ages.

Strain softening region: The softening region is characterized by the softening energy ($G_{f,b}$) and the results are shown in Fig. 26. The values for $G_{f,b}$ increased marginally from 25.6 kJ/m^2 to 27.8 kJ/m^2 for U-S3 and from 21.8 to 23.3 kJ/m^2 for U-H2. Whereas significant increase from 25.5 kJ/m^2 to 33.8 kJ/m^2 was obtained for U-T2. For U-S2 $G_{f,b}$ decreased from 22.1 kJ/m^2 to 15.9 kJ/m^2 due to unusual drops in stress values in some specimens (see Fig. 18 (a)).

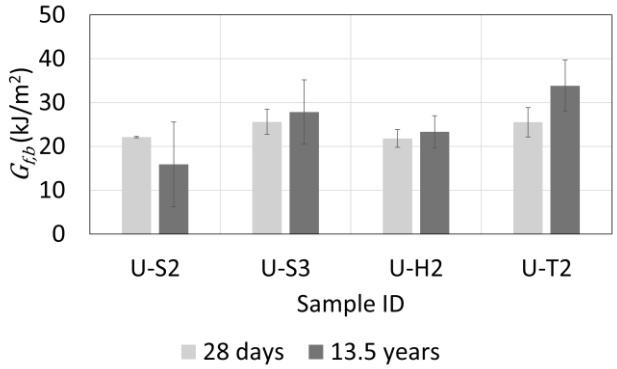

Fig. 26. Softening energy for specimens tested at different ages.

Chapter 4: Conclusions and Recommendations

As a part of this study, the pullout behavior of existing commercial fibers in the US market alongside a newly proposed geometry termed "bundled fibers" in the UHPC matrix were studied. Furthermore, the tensile behavior of UHPC was studied for wide range of commercial fibers and fiber efficiency and fiber utilization factors were defined. Finally, the long term tensile properties of UHPC was studied. Following are the conclusions of these studies:

1. Single fiber pullout behavior: Single-fiber pullout tests indicate that fibers with mechanical anchorage and longer embedment lengths exhibit improved pullout behavior and higher degrees of utilization. Fibers with lower tensile strength also showed higher utilization due to reduced underutilization. The newly proposed geometry termed bundled fibers showed improved pullout behavior than other geometries of fibers due to straightening effect of twisted bundles during pullout. A new parameter was also derived to calculate the degree of slip hardening for steel fibers. Bundled fibers outperformed all other fiber geometries, exhibiting a higher degree of slip hardening, even surpassing twisted fibers.
2. Tensile behavior of UHPC: All the specimens with different fiber types showed improved tensile behavior with increasing fiber volume. On average across all fiber types, increasing fiber content from 1% to 2% raised cracking stress (σ_{cc}) and composite tensile strength (σ_{pc}) by 18% and 30%, respectively, while a further increase to 3% led to increment of 14% and 17%. This was caused due to improved crack bridging due to higher number of fibers being present in the cracking plane. The fibers with higher aspect ratio (100) showed improved tensile behavior than the fibers with lower aspect ratio (50 to 65). The fibers with different surface texture (STR13, ST13, ST-S13), did not show much difference on average in the values of σ_{cc} and σ_{pc}, showing that the fibers contribution is limited by how much stress can be transferred at the interface rather than its intrinsic tensile strength. Among the fibers having different geometries (ST13, W13, H30, T20, T25), the series H30 and T25 show slightly lower strength values than the series ST13, W13and T20 due to lower aspect ratio of fibers H30 and T25.
3. Fiber efficiency and fiber utilization in UHPC: The value of fiber efficiency factor (e_f) showed decreasing trend with increase in volume fraction of fibers due to the increase in group effect of fibers and fibers have less freedom in aligning with the flow direction.

Aspect ratio of fibers was found to be not affecting e_f suggesting that even a fiber with lower aspect ratios can have high efficiency factors when utilized properly. Fibers with different surface texture and geometry were found to have values of e_f depending on whether the fiber response during pullout could be replicated during tensile testing of specimens or not. Also, e_f values were found to be independent of the fibers tensile strength implying that fiber efficiency depends more on how effectively the fibers engage with the matrix to reach their maximum potential at the specimen level not the fiber tensile strength. With increase in fiber volume fraction, fiber utilization factor (u_f) value decreased due to group reduction of bond at higher volume fraction. The fibers with higher aspect ratio had higher u_f values as fewer fibers are needed to form continuous network, which leads to more effective distribution of stress. Among the fibers with different surface texture and geometry, the fibers with improved bonding, having tensile strength aligning more closely with the actual demand in the matrix showed higher values of u_f. The fibers with higher tensile strength showed lower values of u_f, as most of the tensile strength is not utilized at the specimen level.

4. Long term tensile properties of UHPC: After 13.5 years of curing, both the cracking stress (σ_{cc}) and elastic energy increased with aging due to prolonged hydration of cementitious materials which enhanced fiber-matrix bond. Similarly, the composite tensile strength (σ_{pc}) increased for all specimens, while tensile strain capacity (ε_{pc}) increased for most specimens except one. The increase in σ_{pc} led to increased fiber stress which could also be attributed to maturation of UHPC matrix which strengthened the fiber-matrix bond. Multiple cracking increased, resulting in crack spacing (S_{cr}) of less than 4 mm for all specimens. The softening strain (ε_{soft}) and residual strain (ε_{res}) followed trends similar to ε_{pc}, contributing to higher energy absorption capacity (g). Most specimens exhibited increased fracture energy ($G_{f,b}$), though the increment was less than that observed in the energy absorption capacity (g).

References

[1] ASCE, "A Comprehensive Assessment of America's Infrastructure," 2025.

[2] J. 'McBride, N. 'Berman, and A. 'Siripurapu, "The State of U.S. Infrastructure," *Council on Foreign relations*, 2023.

[3] K. Wille, S. El-Tawil, and A. E. Naaman, "Properties of strain hardening ultra high performance fiber reinforced concrete (UHP-FRC) under direct tensile loading," *Cem Concr Compos*, vol. 48, pp. 53–66, 2014, doi: https://doi.org/10.1016/j.cemconcomp.2013.12.015.

[4] ASTM C109/C109M, "Standard Test Method for Compressive Strength of Hydraulic Cement Mortars." doi: 10.1520/C0109_C0109M-20.

[5] S. Pyo, K. Wille, S. El-Tawil, and A. E. Naaman, "Strain rate dependent properties of ultra high performance fiber reinforced concrete (UHP-FRC) under tension," *Cem Concr Compos*, vol. 56, pp. 15–24, 2015, doi: https://doi.org/10.1016/j.cemconcomp.2014.10.002.

[6] M. Dahal and K. Wille, "Slip hardening behavior of bundled steel fibers in ultra-high performance concrete," *Cem Concr Compos*, vol. 155, p. 105844, 2025, doi: https://doi.org/10.1016/j.cemconcomp.2024.105844.

[7] A. E. Naaman, "Engineered steel fibers with optimal properties for reinforcement of cement composites," *Journal of advanced concrete technology*, vol. 1, no. 3, pp. 241–252, 2003.

[8] K. W. and A. E. Naaman, "Effect of Ultra-High-Performance Concrete on Pullout Behavior of High-Strength Brass-Coated Straight Steel Fibers," *ACI Mater J*, vol. 110, no. 4, doi: 10.14359/51685792.

[9] J.-J. Kim and D.-Y. Yoo, "Effects of fiber shape and distance on the pullout behavior of steel fibers embedded in ultra-high-performance concrete," *Cem Concr Compos*, vol. 103, pp. 213–223, 2019, doi: https://doi.org/10.1016/j.cemconcomp.2019.05.006.

[10] Z. Wu, K. H. Khayat, and C. Shi, "How do fiber shape and matrix composition affect fiber pullout behavior and flexural properties of UHPC?," *Cem Concr Compos*, vol. 90, pp. 193–201, 2018, doi: https://doi.org/10.1016/j.cemconcomp.2018.03.021.

[11] D.-Y. Yoo, J.-J. Park, and S.-W. Kim, "Fiber pullout behavior of HPFRCC: Effects of matrix strength and fiber type," *Compos Struct*, vol. 174, pp. 263–276, 2017, doi: https://doi.org/10.1016/j.compstruct.2017.04.064.

[12] E. Zīle and O. Zīle, "Effect of the fiber geometry on the pullout response of mechanically deformed steel fibers," *Cem Concr Res*, vol. 44, pp. 18–24, 2013, doi: https://doi.org/10.1016/j.cemconres.2012.10.014.

[13] K. W. and A. E. Naaman, "Pullout Behavior of High-Strength Steel Fibers Embedded in Ultra-High-Performance Concrete," *ACI Mater J*, vol. 109, no. 4, doi: 10.14359/51683923.

[14] K.-Q. Yu, J.-G. Dai, Z.-D. Lu, and C.-S. Poon, "Rate-dependent tensile properties of ultra-high performance engineered cementitious composites (UHP-ECC)," *Cem Concr Compos*, vol. 93, pp. 218–234, 2018, doi: https://doi.org/10.1016/j.cemconcomp.2018.07.016.

[15] A. Le Hoang and E. Fehling, "Influence of steel fiber content and aspect ratio on the uniaxial tensile and compressive behavior of ultra high performance concrete," *Constr Build Mater*, vol. 153, pp. 790–806, 2017, doi: https://doi.org/10.1016/j.conbuildmat.2017.07.130.

[16] S. El-Tawil, “High Bond Steel Fibers for Ultra High-Performance Concrete (UHPC),” 2022.
[17] V. C. Li, T. Horikoshi, A. Ogawa, S. Torigoe, and T. Saito, “Micromechanics-based durability study of polyvinyl alcohol-engineered cementitious composite,” *Materials Journal*, vol. 101, no. 3, pp. 242–248, 2004.
[18] J. Yu *et al.*, “Tensile performance of sustainable Strain-Hardening Cementitious Composites with hybrid PVA and recycled PET fibers,” *Cem Concr Res*, vol. 107, pp. 110–123, 2018.
[19] L.-Y. Xu, B.-T. Huang, Q. Lan-Ping, and J.-G. Dai, “Enhancing long-term tensile performance of Engineered Cementitious Composites (ECC) using sustainable artificial geopolymer aggregates,” *Cem Concr Compos*, vol. 133, p. 104676, 2022.
[20] A. Naaman, “High Performance Fiber Reinforced Cement Composites,” in *High-performance Construction Materials. Science and Applications*, 2008, pp. 91–153. doi: 10.1142/9789812797360_0003.

Appendix

Table A-1. Summary of pullout parameters of bundled fibers.

Fiber type	Embedment length, l_e (mm)	Maximum Pullout load, P_{max} (N)	Maximum fiber stress, $\sigma_{f,max}$ (MPa)	Average bonding strength (MPa)	Pullout energy, W_p (N-mm)	Slip capacity (mm)
B2	3.3	49.1(±5.6)	781.6(±88.4)	12.6(±1.5)	86.5(±15.7)	1.4(±0.4)
	4.9	75.4(±38.8)	1199.7(±618.1)	13.2(±6.9)	222.5(±110.7)	2.1(±0.7)
	6.5	105.5(±19.3)	1678.3(±307.1)	13.4(±2.6)	431.9(±83.0)	2.7(±1.1)
B3	3.3	87.2(±4.3)	924.7(±46.1)	20.6(±1.2)	111.7(±5.8)	0.8(±0.1)
	4.9	118.5(±18.3)	1304.3(±194.2)	18.9(±2.8)	245.1(±61.2)	1.5(±0.3)
	6.5	180.2(±8.4)	1912.3(±89.6)	20.2(±1.7)	549.5(±80.7)	2.0(±0.4)
B4	3.3	111.5(±6.7)	887.6(±53.0)	21.3(±1.5)	142.5(±6.3)	0.9(±0.2)
	4.9	138.8(±10.3)	1104.3(±82.1)	18.7(±1.8)	255.9(±12.7)	1.0(±0.1)
	6.5	197.2(±50.8)	1569.1(±404.6)	20.1(±4.3)	615.4(±203.8)	2.1(±0.3)
B5	3.3	130.9(±11.8)	833.1(±75.1)	22.3(±0.9)	185.7(±30.8)	1.0(±0.1)
	4.9	196.3(±24.4)	1250.0(±155.2)	24.3(±3.5)	340.3(±47.1)	1.1(±0.3)
	6.5	263.4(±37.4)	1676.9(±238.0)	24.0(±2.9)	754.4(±179.6)	2.0(±0.5)

Table A-2. Summary of pullout parameters of commercial fibers.

Fiber type	Fiber tensile strength, σ_t (MPa)	l_e (mm)	P_{max} (N)	$\sigma_{f,max}$ (MPa)	W_p (N-mm)	$\sigma_{f,max}/\sigma_t$ (in %)
STR10	2850	5	36.3 (± 14.4)	1154.5 (± 456.8)	62.1 (± 21.9)	41
STR13	2850	6.5	44.1 (± 5.5)	1402.3 (± 174.2)	83.6 (± 22.5)	49
STR20	2850	10	62.7 (± 1.4)	1994.8 (± 43.8)	155.9 (± 33.8)	70
ST13	2850	6.5	31.2 (± 8.6)	992.3 (± 273.6)	117.0 (± 29.3)	35
ST-S13	1310	6.5	25.6 (± 2.1)	815.2 (± 65.4)	93.1 (± 3.1)	62
W13	2800	6.5	34.2 (± 3.4)	1087.1 (± 109.5)	147.3 (± 18.4)	39
H30	1345	15	253.4 (± 11.9)	1066.5 (± 50.2)	1108.2 (± 113.1)	79
T20	2900	6.5	153.3 (± 22.1)	2168.3 (± 312.5)	454.5 (± 50.2)	75
T25	1700	6.5	303.6 (± 11.6)	1546.1 (± 59.2)	766.1 (± 53.6)	91

Table A-3. Summary of tensile parameters of UHPC and corresponding fiber efficiency and fiber utilization factors.

Identifier	V_f (%)	$\frac{l_f}{d_f}$	σ_{cc} (MPa)	σ_{pc} (MPa)	ε_{pc} (%)	G_f (KJ/m^2)	$G_{f,b}$ (KJ/m^2)	$G_{f,b}$ (N-mm)	N_f (counted)	W_p (N-mm)	e_f	u_f
STR10	1	50	7.2 (±1.6)	7.7 (±1.4)	0.05 (±0.01)	11.5 (±2.1)	10.9 (±2.0)	5610.5 (±1029.4)	103	62.1 (±21.9)	0.67 (±0.15)	0.32 (±0.06)
	2	50	9.3 (±1.1)	11.1 (±0.7)	0.14 (±0.04)	16.6 (±2.2)	15.5 (±2.2)	7982.0 (±1158.3)	216	62.1 (±21.9)	0.57 (±0.13)	0.22 (±0.01)
	3	50	9.4 (±1.4)	12.0 (±1.2)	0.17 (±0.07)	20.3 (±8.8)	18.9 (±8.4)	9755.7 (±4359.8)	292	62.1 (±21.9)	0.53 (±0.22)	0.16 (±0.02)
STR13	1	65	7.8 (±0.7)	9.9 (±0.5)	0.19 (±0.13)	15.1 (±2.7)	13.8 (±2.4)	7110.1 (±1235.6)	114	83.6 (±22.5)	0.74 (±0.10)	0.39 (±0.02)
	2	65	9.2 (±1.0)	12.6 (±1.2)	0.27 (±0.08)	24.4 (±5.9)	22.3 (±5.1)	11509.2 (±2630.0)	216	83.6 (±22.5)	0.63 (±0.10)	0.24 (±0.02)
	3	65	12.9 (±1.0)	15.6 (±1.1)	0.17 (±0.03)	26.8 (±1.4)	24.9 (±1.3)	12843.5 (±658.8)	290	83.6 (±22.5)	0.53 (±0.05)	0.19 (±0.01)
STR20	1	100	9.8 (±0.9)	12.0 (±1.2)	0.65 (±0.14)	27.5 (±5.9)	22.3 (±5.7)	11501.5 (±2955.8)	130	155.9 (±33.8)	0.62 (±0.16)	0.47 (±0.05)
	2	100	11.6 (±1.3)	16.7 (±0.8)	0.56 (±0.07)	42.9 (±8.8)	38.4 (±8.1)	19844.7 (±4193.7)	255	155.9 (±33.8)	0.50 (±0.09)	0.32 (±0.02)
	3	100	13.6 (±1.5)	19.5 (±1.8)	0.45 (±0.07)	49.7 (±7.9)	46.3 (±8.0)	23884.8 (±4109.6)	367	155.9 (±33.8)	0.42 (±0.03)	0.25 (±0.02)
ST13	1	65	7.4 (±0.6)	7.6 (±0.5)	0.04 (±0.03)	17.6 (±3.2)	17.4 (±3.0)	8995.7 (±1571.1)	119	117.0 (±29.3)	0.65 (±0.12)	0.30 (±0.02)
	2	65	10.0 (±1.8)	11.5 (±2.0)	0.29 (±0.23)	23.8 (±1.2)	19.7 (±3.1)	10180.6 (±1609.1)	210	117.0 (±29.3)	0.46 (±0.08)	0.22 (±0.04)
	3	65	12.8 (±0.6)	15.1 (±1.7)	0.21 (±0.23)	33.3 (±9.9)	29.9 (±6.6)	15432.4 (±3395.6)	307	117.0 (±29.3)	0.43 (±0.06)	0.20 (±0.02)
ST-NC13	1	65	10.3 (±0.7)	10.4 (±0.7)	0.02 (±0.00)	20.7 (±1.8)	20.6 (±1.7)	10623.0 (±861.1)	115	93.1 (±3.1)	0.91 (±0.08)	0.88 (±0.06)
	2	65	11.7 (±1.1)	13.3 (±0.5)	0.18 (±0.11)	31.1 (±4.2)	28.7 (±3.6)	14830.0 (±1833.9)	209	93.1 (±3.1)	0.77 (±0.11)	0.56 (±0.02)
	3	65	12.0 (±1.1)	14.4 (±0.8)	0.27 (±0.17)	31.9 (±5.3)	29.5 (±4.4)	15245.2 (±2290.8)	265	93.1 (±3.1)	0.62 (±0.12)	0.41 (±0.02)
W13	1	65	10.9 (±0.8)	11.2 (±0.5)	0.07 (±0.09)	26.0 (±6.4)	25.3 (±6.4)	13051.4 (±3299.0)	123	147.3 (±18.4)	0.71 (±0.12)	0.45 (±0.02)
	2	65	12.1 (±0.9)	14.1 (±0.9)	0.20 (±0.07)	27.0 (±1.5)	24.7 (±1.1)	12735.2 (±558.1)	226	147.3 (±18.4)	0.38 (±0.03)	0.28 (±0.02)
	3	65	13.2 (±1.6)	16.4 (±2.0)	0.22 (±0.10)	32.2 (±4.2)	29.8 (±2.9)	15364.7 (±1483.8)	306	147.3 (±18.4)	0.34 (±0.03)	0.22 (±0.03)
H30	1	55	8.6 (±0.9)	8.6 (±0.9)	0.02 (±0.00)	11.3 (±1.1)	11.3 (±1.1)	5853.1 (±575.4)	21	1108.2 (±113.1)	0.26 (±0.06)	0.71 (±0.08)
	2	55	9.4 (±0.5)	10.4 (±0.7)	0.25 (±0.18)	18.9 (±2.2)	16.9 (±1.5)	8731.8 (±756.8)	42	1108.2 (±113.1)	0.19 (±0.03)	0.43 (±0.03)
	3	55	9.8 (±0.6)	12.1 (±1.1)	0.30 (±0.13)	24.3 (±6.2)	21.6 (±6.7)	11165.8 (±3432.3)	56	1108.2 (±113.1)	0.18 (±0.06)	0.33 (±0.03)

Identifier	V_f (%)	$\frac{l_f}{d_f}$	σ_{cc} (MPa)	σ_{pc} (MPa)	ε_{pc} (%)	G_f (KJ/m^2)	$G_{f,b}$ (KJ/m^2)	$G_{f,b}$ (N-mm)	N_f (counted)	W_p (N-mm)	e_f	u_f
T20	1	60	10.3 (±1.1)	11.5 (±0.8)	0.09 (±0.10)	15.4 (±3.2)	14.7 (±3.3)	7589.1 (±1719.4)	70	454.5 (±50.2)	0.24 (±0.04)	0.44 (±0.03)
	2	60	11.1 (±1.1)	12.7 (±1.4)	0.32 (±0.18)	23.7 (±3.2)	20.3 (±2.2)	10495.5 (±1157.3)	102	454.5 (±50.2)	0.23 (±0.01)	0.24 (±0.03)
	3	60	12.4 (±0.7)	15.0 (±0.9)	0.32 (±0.06)	28.6 (±4.6)	25.3 (±4.3)	13078.2 (±2203.7)	135	454.5 (±50.2)	0.22 (±0.04)	0.19 (±0.01)
T25	1	50	7.9 (±1.3)	8.7 (±0.7)	0.27 (±0.34)	17.3 (±6.1)	15.4 (±4.4)	7933.5 (±2266.8)	26	766.1 (±53.6)	0.39 (±0.06)	0.57 (±0.05)
	2	50	9.3 (±1.0)	11.2 (±0.8)	0.20 (±0.18)	23.2 (±5.9)	20.9 (±5.3)	10792.1 (±2756.8)	45	766.1 (±53.6)	0.31 (±0.05)	0.36 (±0.02)
	3	50	9.9 (±0.4)	12.8 (±1.2)	0.25 (±0.11)	27.1 (±3.0)	25.1 (±2.0)	12949.0 (±1007.2)	75	766.1 (±53.6)	0.23 (±0.01)	0.28 (±0.03)

Table A-4. Summary of long term tensile properties of UHPC.

Age of specimens	Notation	σ_{cc} (MPa)	g_e (kJ/m^3)	σ_{pc} (MPa)	ε_{pc} (%)	$\sigma_{fpc,avg}$ (MPa)	$\lambda\tau_{eq}$ (MPa)	g (kJ/m^3) exp	g (kJ/m^3) Model	S_{cr} (mm)	$G_{f,b}$ (kJ/m^2)
28 days [3]	U-S2	11.8 (±0.5)	1.2 (±0.1)	15.0 (±0.4)	0.39 (±0.12)	831 (±21.4)	11.5 (±0.3)	67.0 (±13.4)	62.4	4.6	22.1 (±0.2)
	U -S3	12.5 (±1.6)	1.3 (±0.3)	17.8 (±2.1)	0.45 (±0.06)	658 (±78.1)	9.1 (±1.1)	80.0 (±10.7)	72.0	3.2	25.6 (±2.9)
	U -H2	9.4 (±1.4)	0.7 (±0.2)	14.7 (±1.3)	0.48 (±0.03)	815 (±70.0)	9.3 (±0.8)	73.5 (±12.1)	65.9	5.8	21.8 (±2.0)
	U -T2[a]	10.9 (±0.8)	1.0 (±0.1)	14.2 (±0.9)	0.44 (±0.09)	790 (±51.9)	11.9 (±0.8)	68.8 (±11.5)	62.4	4.0	19.5 (±2.5)
	U -T2[b]	13.0 (±0.9)	1.4 (±0.2)	18.6 (±1.2)	0.57 (±0.12)	1032 (±67.8)	11.1 (±0.7)	112.8 (±19.1)	102.6	2.4	25.5 (±3.3)
13.5 years	U -S2	14.6 (±1.6)	1.8 (±0.6)	16.7 (±1.5)	0.33 (±0.22)	929 (±85.7)	12.9 (±1.2)	38.7 (±20.2)	53.4	3.6	15.9 (±9.7)
	U -S3	18.9 (±2.0)	3.2 (±0.7)	22.3 (±3.4)	0.55 (±0.13)	825 (±125.0)	11.4 (±1.7)	119.2 (±42.3)	116.6	2.8	27.8 (±7.3)
	U -H2	14.1 (±0.7)	1.8 (±0.3)	17.0 (±1.3)	0.81 (±0.29)	943 (±72.7)	10.8 (±0.8)	131.3 (±11.0)	155.4	3.7	23.3 (±3.7)
	U -T2	17.3 (±2.6)	2.4 (±0.7)	23.6 (±3.6)	0.89 (±0.17)	1308 (±197.4)	14.7 (±2.2)	175.5 (±45.0)	184.9	2.1	33.8 (±5.9)

[a] Experimental data from ref [3].
[b] adjusted values following the results from ref [5].

Transportation Infrastructure Durability Center
AT THE UNIVERSITY OF MAINE

35 Flagstaff Road
Orono, Maine 04469
tidc@maine.edu
207.581.4376

www.tidc-utc.org